JAERI-M
92-086

DBTT MEASUREMENT BY USE OF SMALL PUNCH (SP) TEST

June 1992

Masahide SUZUKI, Kiyoshi FUKAYA
Yutaka NISHIYAMA and Motokuni ETO

日本原子力研究所
Japan Atomic Energy Research Institute

JAERI-M レポートは，日本原子力研究所が不定期に公刊している研究報告書です。

入手の問合わせは，日本原子力研究所技術情報部情報資料課（〒319－11茨城県那珂郡東海村）あて，お申しこしください。なお，このほかに財団法人原子力弘済会資料センター（〒319-11茨城県那珂郡東海村日本原子力研究所内）で複写による実費頒布をおこなっております。

JAERI-M reports are issued irregularly.

Inquiries about availability of the reports should be addressed to Information Division, Department of Technical Information, Japan Atomic Energy Research Institute, Tokai-mura, Naka-gun, Ibaraki-ken 319-11, Japan.

編集兼発行　日本原子力研究所
印　　刷　日立高速印刷株式会社

DBTT Measurement by Use of Small Punch (SP) Test

Masahide SUZUKI, Kiyoshi FUKAYA , Yutaka NISHIYAMA
and Motokuni ETO

Department of High Temperature Engineering
Tokai Research Establishment
Japan Atomic Energy Research Institute
Tokai-mura, Naka-gun, Ibaraki-ken

(Received May 15, 1992)

Microhardness and SP tests were conducted to improve the reliability of DBTT shift evaluation caused by aging (thermal aging, neutron irradiation, cold rolling) using several model alloys (Fe-0.15C alloys and 2 $^{1}/_{4}$ Cr-1Mo steels).

Although evaluation of DBTT by the SP test was overall good, intergranular brittleness could not be detected by SP DBTT measurement only. By combining other measurements like fractographic observation, however, material degradation can be evaluated more properly.

Keywords : Small Punch Test, Fe-0.15C Alloy, 2 $^{1}/_{4}$ Cr-1Mo Steel, DBTT, Microhardness, Intergranular Fracture, Neutron Irradiation, Temper Embrittlement, Transgranular Fracture, Fractography

SP試験によるDBTT評価

日本原子力研究所東海研究所高温工学部
鈴木　雅秀・深谷　　清・西山　裕孝・衛藤　基邦

(1992年5月15日受理)

微小試験片による延性脆性遷移温度（DBTT）の評価法について，スモールパンチ（SP）試験を中心に検討を行った。熱時効，冷間加工，中性子照射を行った2¼Cr－1Mo鋼及び鉄基モデル合金を用い，SP試験によるDBTT評価の課題を検討した結果，SPDBTTとシャルピー試験によるDBTTは全般的には良い相関が得られた。しかしながら，粒界脆化型のDBTTの上昇に関しては，SP試験片の破壊破面観察等を組み合わせることにより，脆化のより的確な判断を行っていく必要があることが判った。

東海研究所：〒319－11　茨城県那珂郡東海村白方字白根2－4

Contents

1. Introduction 1
2. Experimental Procedure 2
2.1 Materials 2
2.2 Microhardness and Small Punch Tests 2
3. Results and Discussion 3
3.1 Temperature Dependence of Microhardness-related Properties 3
3.2 Temperature Dependence of SP-related Properties 4
3.3 Factors Affecting the Temperature Dependence of Pmax 4
3.4 Reliable Detection of Material Degradation in
Terms of DBTT Shift 8
4. Conclusion 9
Acknowledgement 10
References 11
Appendix 20

目　　次

1. 序 …… 1
2. 実験方法 …… 2
2.1 材　料 …… 2
2.2 微小硬さ及びスモールパンチ（SP）試験 …… 2
3. 実験結果及び考察 …… 3
3.1 微小硬さの試験温度依存性 …… 3
3.2 SP特性の温度依存性 …… 4
3.3 Pmaxの温度依存性に及ぼす影響因子 …… 4
3.4 DBTT変化のより信頼性ある検出について …… 8
4. 結　論 …… 9
謝　辞 …… 10
参考文献 …… 11
付　録 …… 20

1. Introduction

Although small specimen technique is necessary to evaluate the radiation response of materials not only for fusion but also fission reactors from the point of improving availability of surveillance test specimens, fracture-related properties like fracture toughness, ductile brittle transition temperature (DBTT) and so on are difficult to measure by small and/or limited number of specimens. Considering that these properties are key factors for assessing the structural integrity of nuclear reactor components, it is essential that small specimen technique aiming at the toughness evaluation be developed. Hardness and bulge tests have methodological advantages because they possess certain flexibility from the standpoint of miniaturization. The former is well known to have a good relation with tensile strength. As an example of the latter method, small punch (SP) test is being successively applied to evaluate the fracture-related properties such as DBTT[1-7].

In the SP test, DBTT determination is conducted based on the temperature dependence of a certain SP-related parameter. SP energy which is defined as an energy consumed during the test before the onset of macrocracking is often used for this parameter. The DBTT determined from SP test (SPDBTT) has a good correlation with Charpy DBTT[1-3]. However, further study is still needed as to whether it can detect and evaluate degradation properly corresponding to various material degradation modes.

In the present paper, improved way of DBTT assessment using SP and microhardness tests is argued.

2. Experimental Procedure

2.1 Materials

Materials used in the present experiment were two kinds of Fe-C alloys with different heat treatment (material C and D) and two kinds of $2^1/_4$Cr-1Mo steels (material NT: normalized and tempered , material AN: annealed). Chemical compositions and heat treatment conditions are shown in Tables 1 and 2. Experiments were also conducted using the NT $2^1/_4$Cr-1Mo steels thermally aged or neutron irradiated or cold worked. Thermal aging was conducted at 723K for 50000h. Neutron irradiation was conducted in Japan Research Reactor-2 (JRR-2) at 573 K to a fluence of 2 x 10^{23}n/m^2 (E>1MeV).

2.2 Microhardness and Small Punch Tests

Microhardness test with a maximum applied load of 100gf (0.98N) was conducted at temperatures from room temperature down to 160 K. During the test, applied load and indentation depth were measured to evaluate hardness-related property accurately.

SP test was performed in the temperature range from 77 K to 300K. Specimens for the SP test were 10 x 10 mm^2 coupons with 0.5 mm thickness. The SP test method and apparatus are presented

In the present paper, improved way of DBTT assessment using SP and microhardness tests is argued.

2. Experimental Procedure

2.1 Materials

Materials used in the present experiment were two kinds of Fe-C alloys with different heat treatment (material C and D) and two kinds of $2^1/_4$Cr-1Mo steels (material NT: normalized and tempered , material AN: annealed). Chemical compositions and heat treatment conditions are shown in Tables 1 and 2. Experiments were also conducted using the NT $2^1/_4$Cr-1Mo steels thermally aged or neutron irradiated or cold worked. Thermal aging was conducted at 723K for 50000h. Neutron irradiation was conducted in Japan Research Reactor-2 (JRR-2) at 573 K to a fluence of 2 x 10^{23}n/m^2 (E>1MeV).

2.2 Microhardness and Small Punch Tests

Microhardness test with a maximum applied load of 100gf (0.98N) was conducted at temperatures from room temperature down to 160 K. During the test, applied load and indentation depth were measured to evaluate hardness-related property accurately.

SP test was performed in the temperature range from 77 K to 300K. Specimens for the SP test were 10 x 10 mm^2 coupons with 0.5 mm thickness. The SP test method and apparatus are presented elsewhere[4,5]. A hard steel ball with 2.4 mm diameter was used for the punching. All SP tests were performed at a crosshead speed of 8.3×10^{-3} mm/s.

3. Results and Discussion

3.1 Temperature Dependence of Microhardness-related Properties

Hardness-related properties can be evaluated well by analyzing load versus indentation depth relationship[8]. For example, this relationship obtained during loading can be expressed in the following way;

$$L/d = A_0 + A_1 * d \qquad (1)$$

where L is load, d is indentation depth, and A_0 and A_1 are constants. Suzuki et al. showed that constant A_1 has a linear relationship with yield or tensile strength[7]. Although various attempts were made to detect the temperature dependence of a certain microhardness-related parameter which could be correlated with ductile to brittle transition behavior, any of these could not be correlated with fracture-related property like DBTT in the present experiment. Fig.1 shows A_1 as a function of test temperature for NT $2^1/_4$Cr-1Mo steels of as received and 80% cold worked. As the test temperature decreases, A_1 for both materials increased in a similar manner.

elsewhere[4,5]. A hard steel ball with 2.4 mm diameter was used for the punching. All SP tests were performed at a crosshead speed of 8.3×10^{-3} mm/s.

3. Results and Discussion

3.1 Temperature Dependence of Microhardness-related Properties

Hardness-related properties can be evaluated well by analyzing load versus indentation depth relationship[8]. For example, this relationship obtained during loading can be expressed in the following way;

$$L/d = A_0 + A_1 * d \qquad (1)$$

where L is load, d is indentation depth, and A_0 and A_1 are constants. Suzuki et al. showed that constant A_1 has a linear relationship with yield or tensile strength[7]. Although various attempts were made to detect the temperature dependence of a certain microhardness-related parameter which could be correlated with ductile to brittle transition behavior, any of these could not be correlated with fracture-related property like DBTT in the present experiment. Fig.1 shows A_1 as a function of test temperature for NT $2^1/_4$Cr-1Mo steels of as received and 80% cold worked. As the test temperature decreases, A_1 for both materials increased in a similar manner.

3.2 Temperature Dependence of SP-related Properties

Fig. 2 shows SP-related properties (SP_{energy}, δ^*, P_{max}) of Fe-0.15C alloys (material C and D) as a function of SP test temperature. Here, δ^* is maximum deflection at the onset of macrocracking and P_{max} is maximum load during the test (for detailed definition see reference[5]) . P_{max} is normalized by $t_0{}^2$(t_0 is initial specimen thickness). As the test temperature decreases, all these SP-related values show sudden decrease at a certain temperature. This temperature is thought to correspond to a point where ductile to brittle transition occurs. There is no difference at the point where sudden drop occurs among these properties. Therefore, as maximum load can be measured most easily and thus with less scatter, P_{max} can be used for the parameter to determine the DBTT from the practical aspects in application. In the present paper, P_{max} is used for evaluating DBTT.

3.3 Factors Affecting the Temperature Dependence of P_{max}

(1) Effect of Microstructure

Difference of microstructure can give a clear difference of P_{max} versus test temperature relationship. In Fig.2, the clear difference is seen for Fe-0.15C alloys having a different microstructure (material C and D), where microstructure is ferrite (plus pearlite) for the material C, and bainite for the material

D. Another example is also seen in Fig.3, where P_{max} of two kinds of $2^1/_4$Cr-1Mo steels having a different heat treatment history is shown. The microstructure is ferrite plus pearlite for the material AN (annealed), and bainite (plus proeutectoid ferrite) for the material NT (normalized and tempered). SP DBTT is very sensitive to complete microstructural change. Fig.4 shows the relationship between SPDBTT and Charpy DBTT. The former is tentatively determined to be a temperature corresponding to half the maximum P_{max}, and the latter is evaluated in terms of 68J absorbed energy. SPDBTT is often correlated with Charpy DBTT by the following equation;

$$\text{SPDBTT} = \alpha * \text{Charpy DBTT} \tag{2}$$

where α is correlation coefficient. Using the materials with different microstructures (ferrite , pearlite), α of about 0.4 could be obtained.

(2) Effect of Hardening (cold rolling and neutron irradiation)

In general, the shift of DBTT caused by neutron irradiation can be explained clearly by the Ludwig-Davidenkov relationship, that is, an increase in yield stress or radiation hardening results in a DBTT shift. Likewise the case of neutron irradiation, cold working also induces a DBTT shift. In Fig.5, $P_{max}/t_o{}^2$ is represented as a function of test temperature for NT $2^1/_4$Cr-1Mo steels of as received, 20% cold worked and 50% cold worked. The material 50% cold worked showed more than 50 K increase of SPDBTT. Interesting feature of the temperature dependence of P_{max}

for cold worked materials is that difference of P_{max} among these three materials becomes less as temperature decreases. That is, ΔP_{max} (= P_{max}(cold worked) - P_{max}(as received)) is largest at room temperature, and tends to be very small as the SP test temperature becomes lower. Similar tendency can be also observed for neutron irradiated materials as shown in Fig.6, where P_{max} of NT $2^1/_4$Cr-1Mo steel before and after irradiation is shown as a function of test temperature. This tendency is a clear contrast to the case when two materials have different microstructure as a result of different heat treatment. ΔP_{max}(for example, = P_{max}(NT) - P_{max}(AN)) is almost constant over entire temperature range down to low temperature (see Figs.2 and 3).

(3) Effect of Intergranular Brittleness

DBTT also increases as a result of intergranular brittleness. Typical example of this case is temper embrittlement which is seen in low alloy steels when they are exposed to the temperature region ranged from ~673K to ~823K. NT $2^1/_4$Cr-1Mo steel also becomes brittle after long term thermal aging. Table 3 shows the Charpy-related properties like DBTT measured by 68J absorbed energy, fracture appearance transition temperature(FATT) and fraction of intergranular fracture for NT $2^1/_4$Cr-1Mo steel before and after 50000 h thermal aging. After 50000 h thermal aging at 723K, the DBTT increased about 40 K, and this shift is accompanied by the increase in the fraction of intergranular fracture. In Fig.7, P_{max} is shown as a function of test temperature. It is to be noted that despite the fact that Charpy DBTT increased, there was no clear difference in SP-related properties. Simple execution of SP test has a possibility to fail to detect the material degradation caused by intergranular brittleness.

(4) Observation of Fracture Surface for SP Specimen

Fracture surface of SP specimen was observed by a scanning electron microscope (SEM). It was ascertained that as the test temperature decreased, fracture mode changed from ductile fracture to brittle fracture mode. Fig.8 shows the fraction of ductile fracture as a function of test temperature for materials already described. The temperature dependence of the fraction of ductile fracture is coincident with that of P_{max}. This fact means that degradation of NT $2^1/_4$Cr-1Mo steels caused by thermal aging (723K x 50000 h) could not be detected using this parameter also. However, from a careful observation, slight difference was seen in the lower fraction of ductile fracture region. That is, the point where the fraction of ductile fracture begins to increase (indicated by an arrow in Fig.8) was higher for the aged material. Furthermore, in the fractographic examination, it was shown that the fracture appearance was greatly changed. Fig.9 shows the scanning electron micrographs of the SP specimen after test (Fig.9(A)) and its typical fracture surface appearance (Fig.9(B-D)) for NT $2^1/_4$Cr-1Mo steel after thermal aging (723K x 50000 h). Test temperature was at 118K (transition region). As is seen in the photographs (B-D), intergranular fracture was clearly seen for this material. By contrast, only small fraction of intergranular fracture was observed in the as received material. Fracture appearance was summarized in Fig.10 for NT $2^1/_4$Cr-1Mo steels before and after the thermal aging. Here, the fractions of intergranular (I.G.), transgranular cleavage (C) and ductile (D) fracture were determined based on about 10 - 20 SEM photographs taken at the magnification of 1000. The fraction of occurrence of intergranular fracture was larger than that of Charpy specimen possibly due to biaxial stress state in the SP test specimen.

3.4 Reliable Detection of Material Degradation in Terms of DBTT Shift

Although clear relationship is seen between Charpy DBTT and SPDBTT from the experiment using the materials of different microstructure, whether this correlation is valid or not for the evaluation of material degradation which will be caused in various manner is still open to question because of the lack of the physical mechanism. Deformation behavior during the SP test can be divided into four regions[1]; Ⅰ.Elastic bending, Ⅱ.Plastic bending, Ⅲ.Plastic membrane stretching, Ⅳ.Plastic instability. As test temperature decreases, the region at which fracture occurs changes from Ⅳ to Ⅰ via Ⅲ and Ⅱ. Material degradation can affect the balance of contribution corresponding to each deformation region. One example was shown in the temperature dependence of P_{max}. P_{max} is constituted by four components corresponding to the four deformation modes;

$$P_{max} = P_{I} + P_{II} + P_{III} + P_{IV} \quad (3)$$

As cold working or neutron irradiation reduces plasticity (elongation), reductions in the constituents of P_{III} and P_{IV} make the total increment (ΔP_{max}) much smaller as the temperature becomes low(in case, it can be negative). Therefore it is apparent there would no clear relationship between P_{max} in SP test and ultimate tensile strength in tensile test when the entire test temperature region is considered. Therefore, for obtaining tensile-related properties, hardness still possess an advantage over SP test. Likewise tensile properties, SP-Charpy DBTT correlation has some limitation. As was shown for thermal aged NT $2^{1}/_{4}$Cr-1Mo steel, mere execution of SP test could not detect DBTT shift. Fractographic observation was absolutely necessary, by which the change of the fracture mode could be detected. The fact that neutron irradiation or hardening-induced DBTT shift can most possibly be detected by the SP test method is very encouraging for the application of the SP test to the material degradation evaluation in nuclear reactor components.

4. Conclusion

Microhardness and SP tests were conducted to improve the reliability of DBTT shift evaluation caused by aging including irradiation using several model alloys (Fe-0.15C alloys and $2^{1}/_{4}$Cr-1Mo steels) which also received thermal aging or neutron irradiation or cold working. Main results obtained were as follows:

$$P_{max} = P_{I} + P_{II} + P_{III} + P_{IV} \qquad (3)$$

As cold working or neutron irradiation reduces plasticity (elongation), reductions in the constituents of P_{III} and P_{IV} make the total increment (ΔP_{max}) much smaller as the temperature becomes low(in case, it can be negative). Therefore it is apparent there would no clear relationship between P_{max} in SP test and ultimate tensile strength in tensile test when the entire test temperature region is considered. Therefore, for obtaining tensile-related properties, hardness still possess an advantage over SP test. Likewise tensile properties, SP-Charpy DBTT correlation has some limitation. As was shown for thermal aged NT $2^{1}/_{4}$Cr-1Mo steel, mere execution of SP test could not detect DBTT shift. Fractographic observation was absolutely necessary, by which the change of the fracture mode could be detected. The fact that neutron irradiation or hardening-induced DBTT shift can most possibly be detected by the SP test method is very encouraging for the application of the SP test to the material degradation evaluation in nuclear reactor components.

4. Conclusion

Microhardness and SP tests were conducted to improve the reliability of DBTT shift evaluation caused by aging including irradiation using several model alloys (Fe-0.15C alloys and $2^{1}/_{4}$Cr-1Mo steels) which also received thermal aging or neutron irradiation or cold working. Main results obtained were as follows:

(1) Maximum load during the SP test (P_{max}) can be used for the parameter to determine the DBTT.

(2) SPDBTT is sensitive to complete microstructural change (ferrite ,pearlite). In this case, SPDBTT-Charpy DBTT correlation coefficient of about 0.4 can be obtained.

(3) SP DBTT shift owing to hardening (cold working and neutron irradiation) can be detected by the temperature dependence of P_{max}, although ΔP_{max} (= P_{max}(cold worked or irradiated) - P_{max}(as received)) is largest at room temperature, and tends to be very small as the SP test temperature becomes lower.

(4) Temper embrittlement of $2^1/_4$Cr-1Mo steel cannot be detected by SP DBTT measurement. In this case, fractographic observation can reveal the change of fracture mode from transgranular to intergranular type.

(5) Microhardness-related parameters could not be correlated with ductile to brittle transition behavior. However, it is still necessary to evaluate material degradation, because it possess an advantage for obtaining tensile-related properties over SP test in entire temperature region.

Acknowledgement

The authors would like to express their sincere gratitude to Dr.T.Kodaira of JAERI for reviewing this manuscript and professors H.Takahashi of Tohoku University and T.Misawa of Muroran Institute of Technology for valuable advices. Dr.S.Jitsukawa of JAERI is also acknowledged for valuable discussion and comments.

(1) Maximum load during the SP test (P_{max}) can be used for the parameter to determine the DBTT.

(2) SPDBTT is sensitive to complete microstructural change (ferrite ,pearlite). In this case, SPDBTT-Charpy DBTT correlation coefficient of about 0.4 can be obtained.

(3) SP DBTT shift owing to hardening (cold working and neutron irradiation) can be detected by the temperature dependence of P_{max}, although ΔP_{max} (= P_{max}(cold worked or irradiated) - P_{max}(as received)) is largest at room temperature, and tends to be very small as the SP test temperature becomes lower.

(4) Temper embrittlement of $2^1/_4$Cr-1Mo steel cannot be detected by SP DBTT measurement. In this case, fractographic observation can reveal the change of fracture mode from transgranular to intergranular type.

(5) Microhardness-related parameters could not be correlated with ductile to brittle transition behavior. However, it is still necessary to evaluate material degradation, because it possess an advantage for obtaining tensile-related properties over SP test in entire temperature region.

Acknowledgement

The authors would like to express their sincere gratitude to Dr.T.Kodaira of JAERI for reviewing this manuscript and professors H.Takahashi of Tohoku University and T.Misawa of Muroran Institute of Technology for valuable advices. Dr.S.Jitsukawa of JAERI is also acknowledged for valuable discussion and comments.

References

[1] Baik,J.M.,Kameda,J. and Buck,O.,"Development of Small Punch Tests for Ductile-Brittle Transition Temperature Measurement of Temper Embrittled Ni-Cr Steels," The Use of Small Scale Specimens for Testing Irradiated Materials, ASTM STP 888,W.R.Corwin and G.E.Lucas,Eds., American Society for Testing and MAterials, Philadelphia,1986,pp92-111.

[2] Misawa,T.,Adachi,T, Saito,M. and Hamaguchi,Y.,"Small Punch Tests for Evaluating Ductile-Brittle Transition Behavior of Irradiated Ferritic Steels",Journal of Nuclear Materials, Vol.150(1987)pp.194-202.

[3] Matsushita,T., Saucedo, M.L.,Yotsutsuji, M,Shoji,T. and Takahashi,H., "Correlation between a Charpy V-notch Impact Test and a Small Punch Test in Ductole-Brittle Fracture Mode Transition Behavior (in Japanese)" Trans. Japan Soc. Mech. Engineers,55-515(1989)pp.1619-1622.

[4] Mao,X., Shoji,T. and Takahashi,H., "Characterization of Fracture Behavior in Small Punch Test by Combined Recrystallization-Etch Method and Rigid Plastic Analysis", J.Testing and Evaluation, Vol.15(1987)pp.30-37.

[5] Takahashi,H., Shoji,T., Mao,X., Hamaguchi,Y., Misawa,T., Saito,M., Oku,T., Kodaira,T., Fukaya,K., Nishi,H. and Suzuki,M., "Recommended Practice for Small Punch (SP) Testing of Netalic Materials (Draft),JAERI-M Report 88-172(1988).

[6] Suzuki,M., Eto,M.,Fukaya,K., Nishiyama,Y.,Kodaira,T.,Oku,T. Adachi,M.,Umino,U.,Takahashi,I.,Misawa,T. and Hamaguchi,Y. "Evaluation of Toughness Degradation by Small Punch (SP) Tests for Neutron Iraadiated $2^1/_4$Cr-1Mo Steel",Journal of Nuclear Materials 179-181(1991)pp.441-444.

[7] Suzuki,M. et al. ,to be published in Journal of Nuclear Materials.

[8] Inamura,M. and Suzuki,T., Seisan-kenkyu (in Japanese),Vol.42, 257(1990)

Table 1 Chemical compositions of the materials used.

Alloy		C	Si	Mn	P	S	Ni	Cr	Cu	Mo
Fe-0.15C	C	0.144	0.02	<0.01	0.032	0.003	<0.01	<0.01	<0.01	<0.01
	D	0.152	0.02	<0.01	0.032	0.003	<0.01	<0.01	<0.01	<0.01
2 1/4Cr-1Mo	NT	0.14	0.08	0.54	0.009	0.009	0.12	2.36	0.09	1.04
	AN	0.13	0.07	0.52	0.009	0.009	0.12	2.32	0.09	1.03

Table 2 Heat treatment conditions of the materials used.

Designation	Treatment Type	Details
NT	normalized and tempered	austenized at 1173/1198K for 5 h, quenching tempered at 913/933K for 6 h, air cooled, PWHT
AN	annealed	austenized at 1173/1198K for 5 h, cooled at a rate of 60K/h, PWHT
C	annealed	austenized at 1153K for 1 h, 100K/h furnace cooling
D	quenched and tempered	austenized at 1153K for 1 h, water quenching, tempered at 913K for 1 h, air cooling

PWHT: 950/963K for 22 h

Table 3 Charpy-related properties of the NT $2^1/_4$ Cr-1Mo steel before and after 50000 h aging at 723K.

NT 2 1/4Cr-1Mo	Charpy-related Properties		
	vTr50	FATT	F.I.F
As received	193K	215K	0 %
723K x 50000h aged	234K	273K	22%

vTr50: 68J absorved energy transition temperature
FATT: 50% fibrosity transition temperature
F.I.F: Fraction of intergranular fracture at lower shelf region

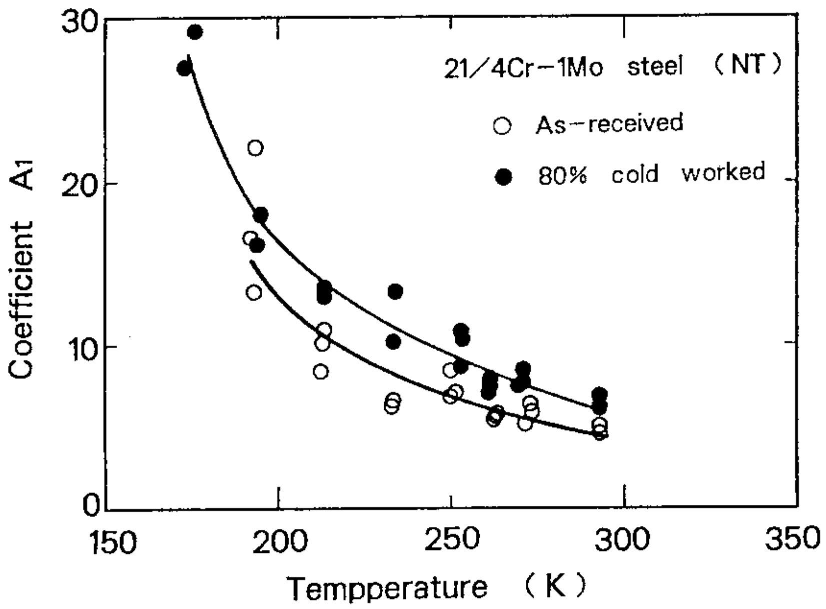

Fig. 1 Microhardness-related property (coefficient A_1) as a function of test temperature for the NT $2^1/_4$ Cr-1Mo steel, as received and 80 % cold worked.

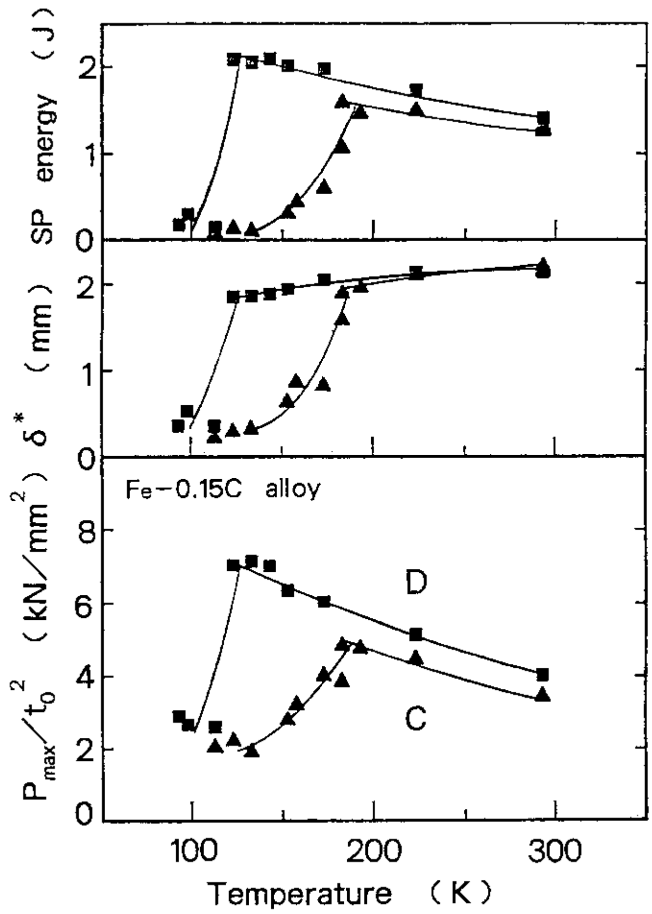

Fig. 2 SP-related properties (SP_{energy}, δ^* and P_{max}) as a function of test temperature

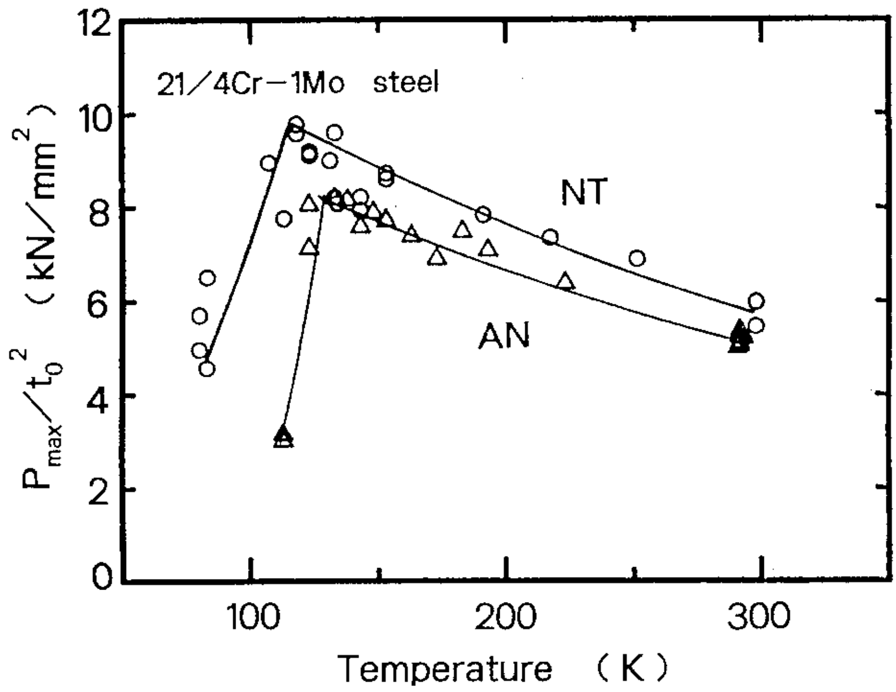

Fig. 3 P_{max}/t_0^2 as a function of the SP test temperature for the NT and AN $2^1/_4$ Cr-1Mo steels.

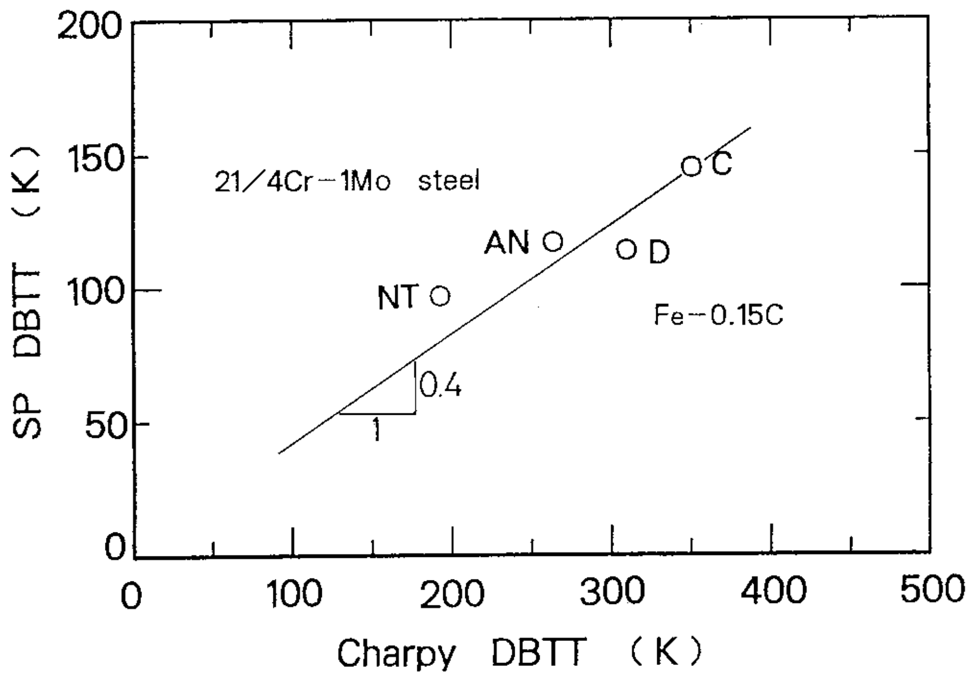

Fig. 4 The relationship between SP DBTT and Charpy DBTT for $2^1/_4$ Cr-1Mo steels and Fe-0.15C alloys.

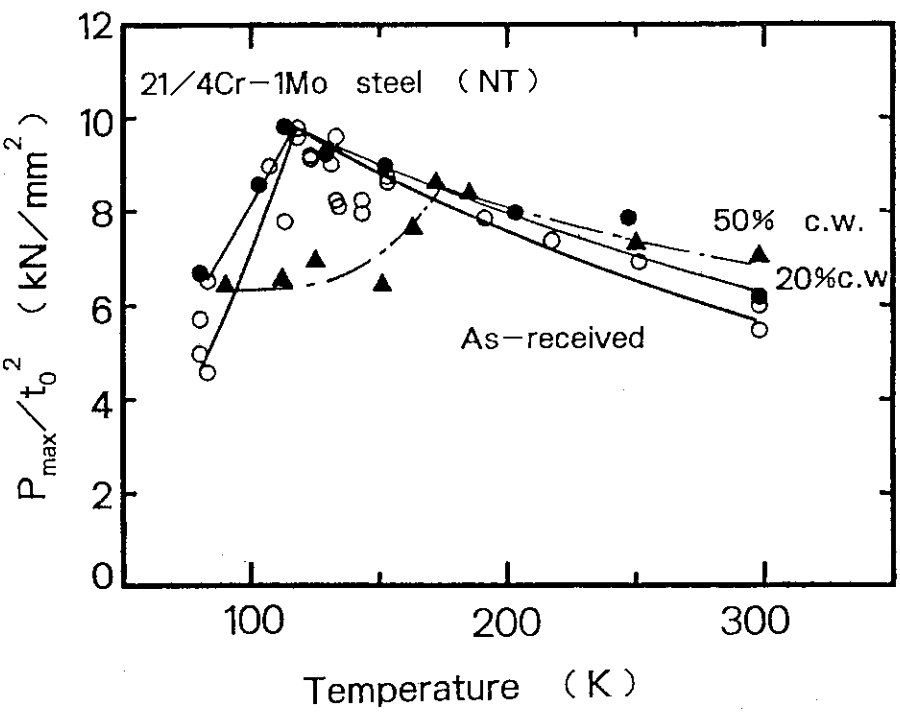

Fig. 5 P_{max}/t_0^2 as a function of the SP test temperature for the NT $2^1/_4$ Cr-1Mo steels after 20 % and 50 % cold working.

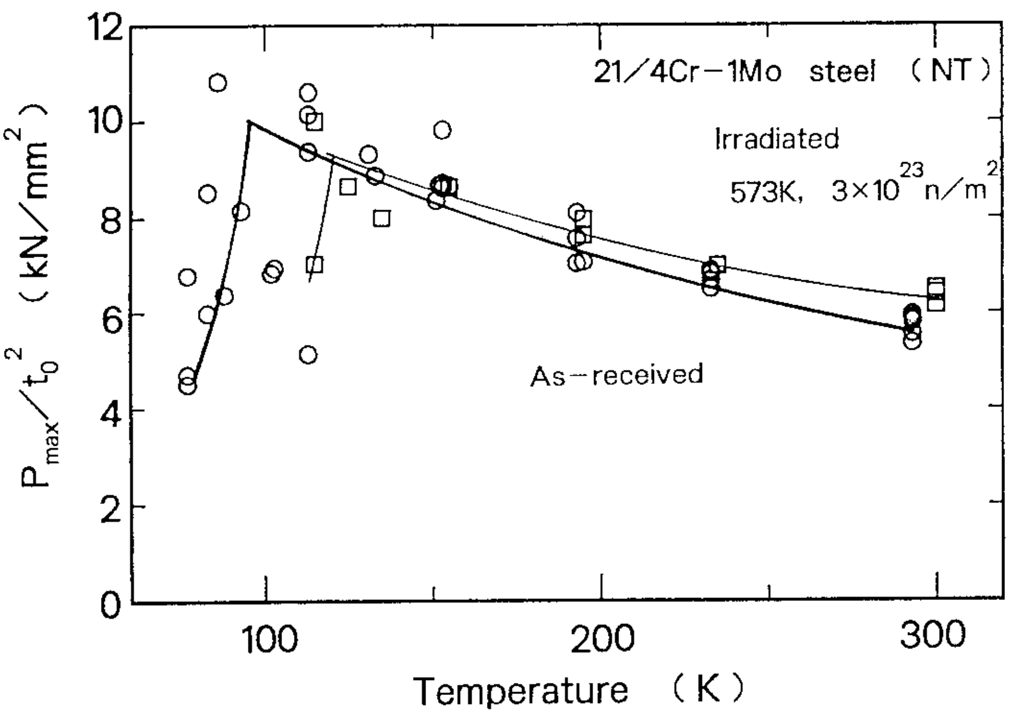

Fig. 6 P_{max}/t_0^2 as a function of the SP test temperature for the NT $2^1/_4$ Cr-1Mo steel before and after neutron irradiation at 573K to the fluence of $3x10^{23}n/m^2$(E>1MeV)

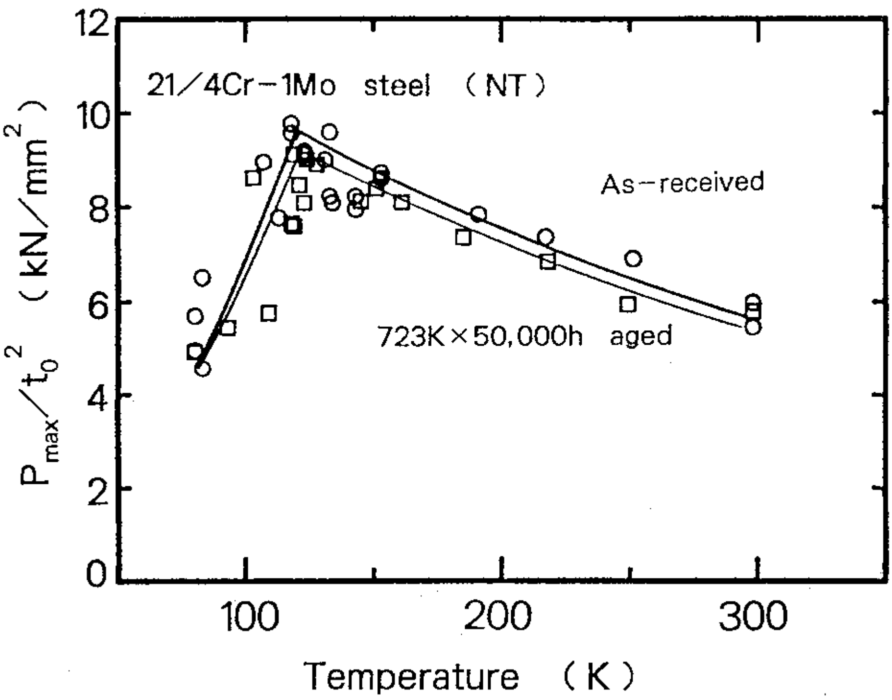

Fig. 7 P_{max}/t_0^2 as a function of the SP test temperature for the NT $2^1/_4$ Cr-1Mo steel before and after thermal aging at 723K for 50000 h.

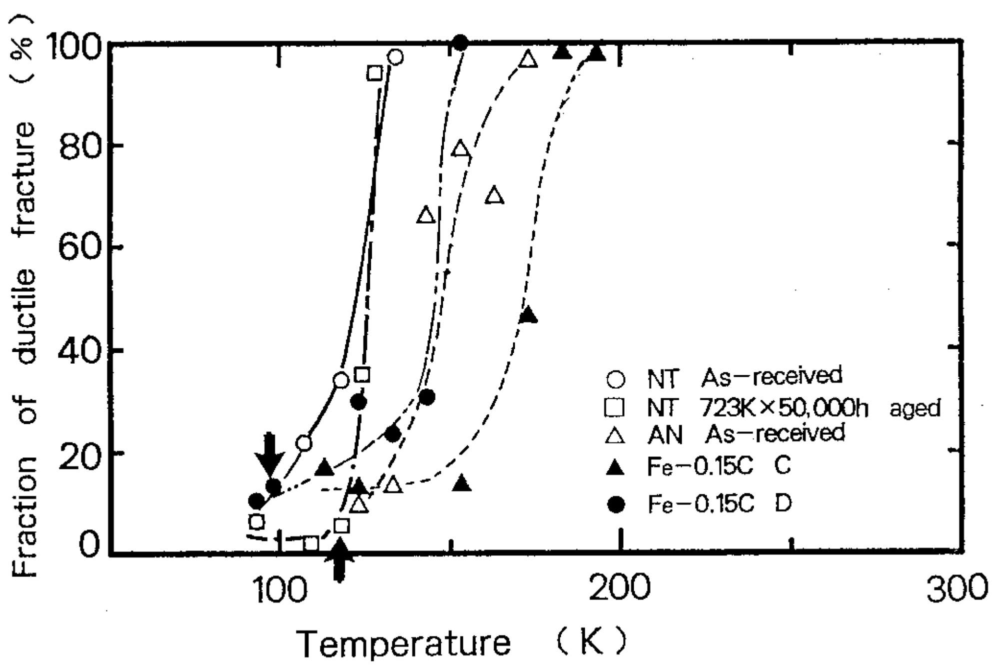

Fig. 8 Fraction of the ductile fracture as a function of the SP test temperature for $2^1/_4$ Cr-1Mo steels and Fe-0.15C alloys.

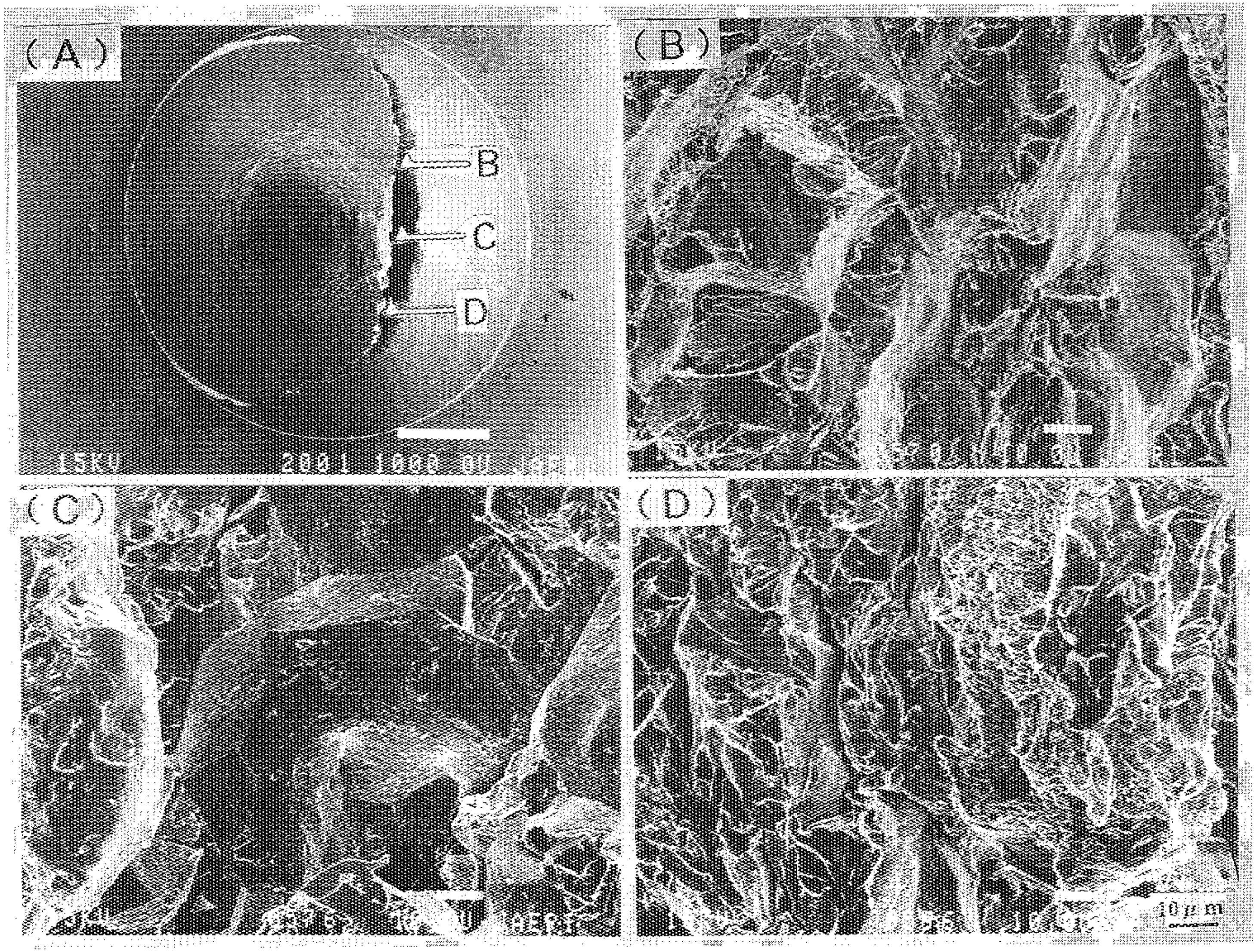

Fig. 9 Scanning electron micrographs of the SP specimen after the test (A), and its typical fracture surface corresponding to location B, C and D (B-D) for $2^1/_4$ Cr-1Mo steel thermally aged at 723K for 50000h, SP test was conducted at 118K.

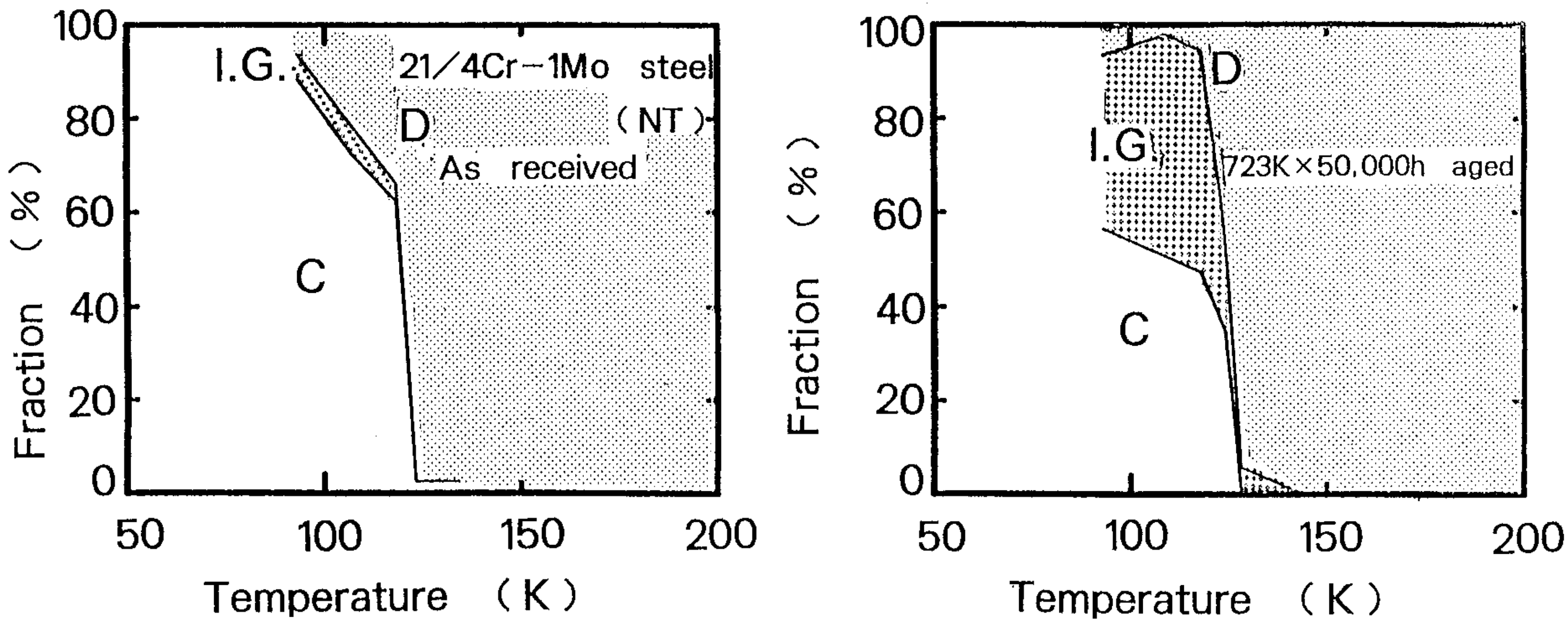

Fig. 10 Fraction of intergranular, transgranular cleavage and ductile fracture in the SP fracture surface as a function of SP test temperature for NT $2^{1}/_{4}$ Cr-1Mo steel before and after thermal aging at 723K for 50000h.

Appendix Fig. 1－10

Appendix Fig. 1
SP-related parameters as a function of test temperature for 2 1/4Cr-1Mo steel(AN,NT).

Appendix Fig. 2
SP-related parameters as a function of test temperature for 2 1/4Cr-1Mo steel (AN,NT,NT aged).

Appendix Fig. 3
SP-related parameters as a function of test temperature for 2 1/4Cr-1Mo steel (LL,HH).

Appendix Fig. 4
SP-related parameters as a function of test temperature for 2 1/4Cr-1Mo steel (HL,LH).

Appendix Fig. 5
SP-related parameters as a function of test temperature for 2 1/4Cr-1Mo steel (LL,HH,HL,LH).

Appendix Fig. 6
SP-related parameters as a function of test temperature for 2 1/4Cr-1Mo steel (cold worked).

Appendix Fig. 7
SP-related parameters as a function of test temperature for 2 1/4Cr-1Mo steel (cold worked).

Appendix Fig. 8
SP-related parameters as a function of test temperature for 2 1/4Cr-1Mo steel (Fe-0.02C(A),Fe-0.02C-0.03P(B)).

Appendix Fig. 9
SP-related parameters as a function of test temperature for 2 1/4Cr-1Mo steel (Fe-0.15C-0.03P(C),Fe-0.15C-0.03P(D)).

Appendix Fig. 10
SP-related parameters as a function of test temperature for 2 1/4Cr-1Mo steel (Fe-0.02C(A),Fe-0.02C-0.03P(B),Fe-0.15C-0.03P(C),Fe-0.15C-0.03P(D)).

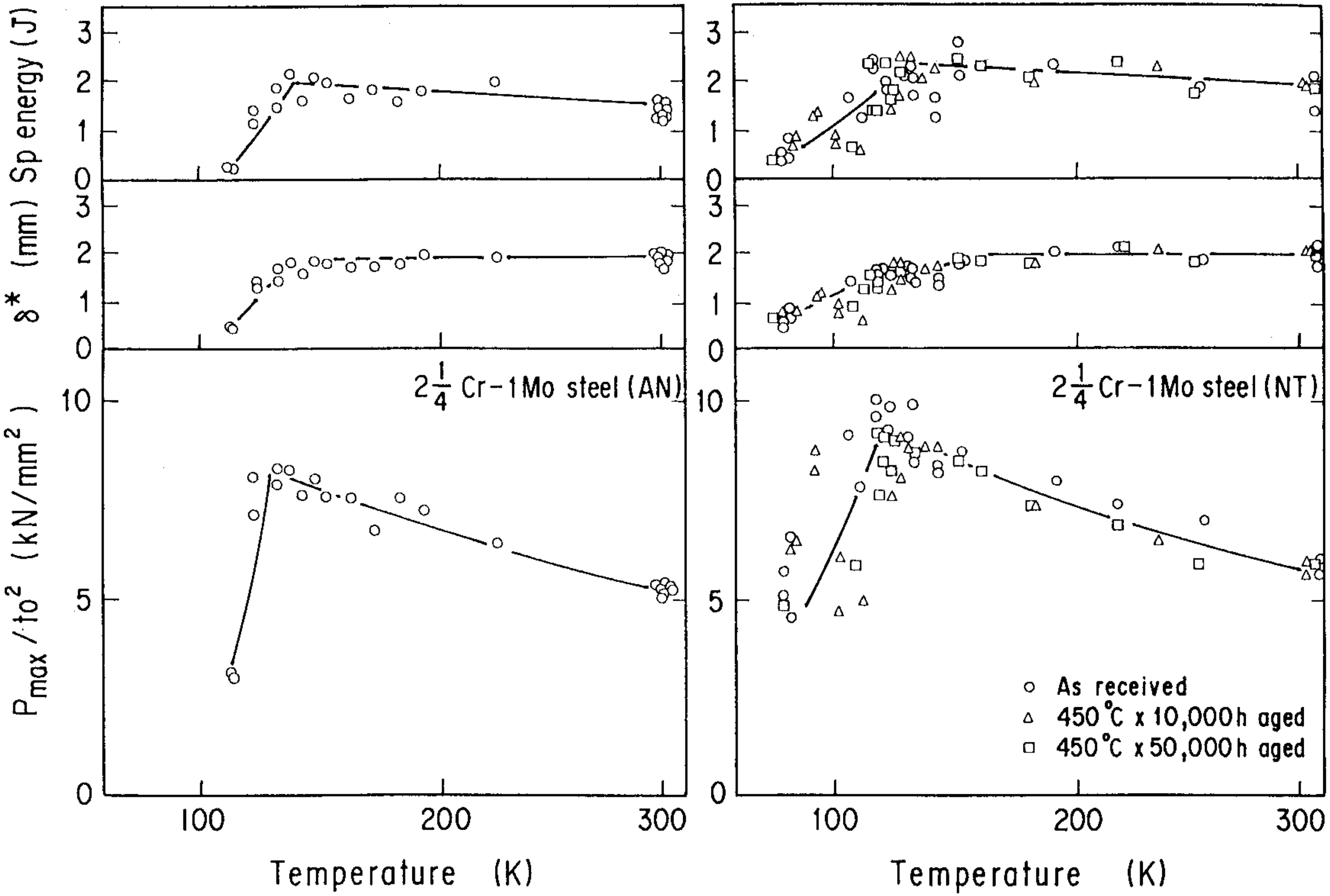

Appendix Fig. 1 SP-related parameters as a function of test temperature for 2 1/4Cr-1Mo steel (AN, NT).

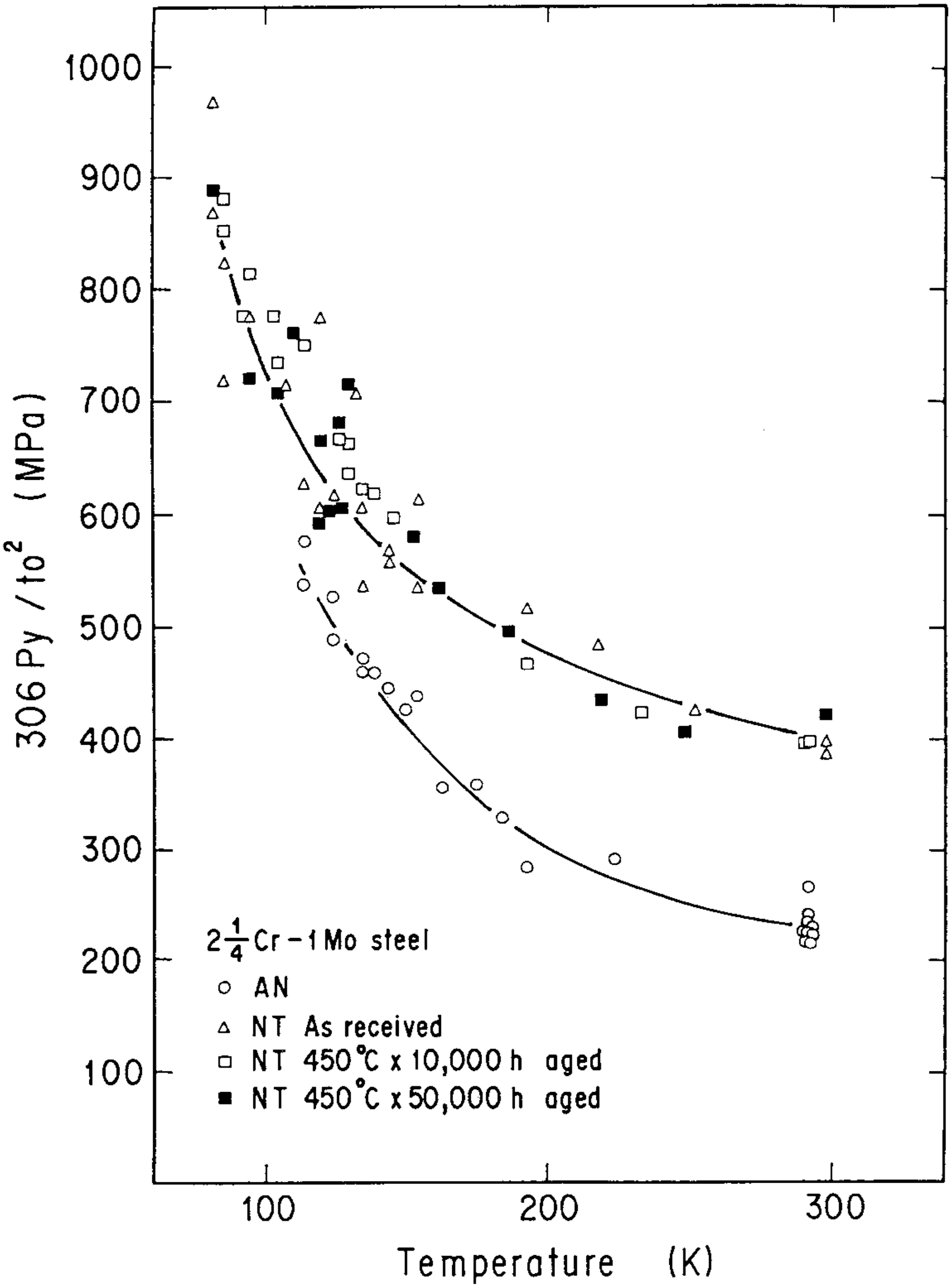

Appendix Fig. 2 SP-related parameters as a function of test temperature for 2 1/4Cr-1Mo steel (AN, NT, NT aged).

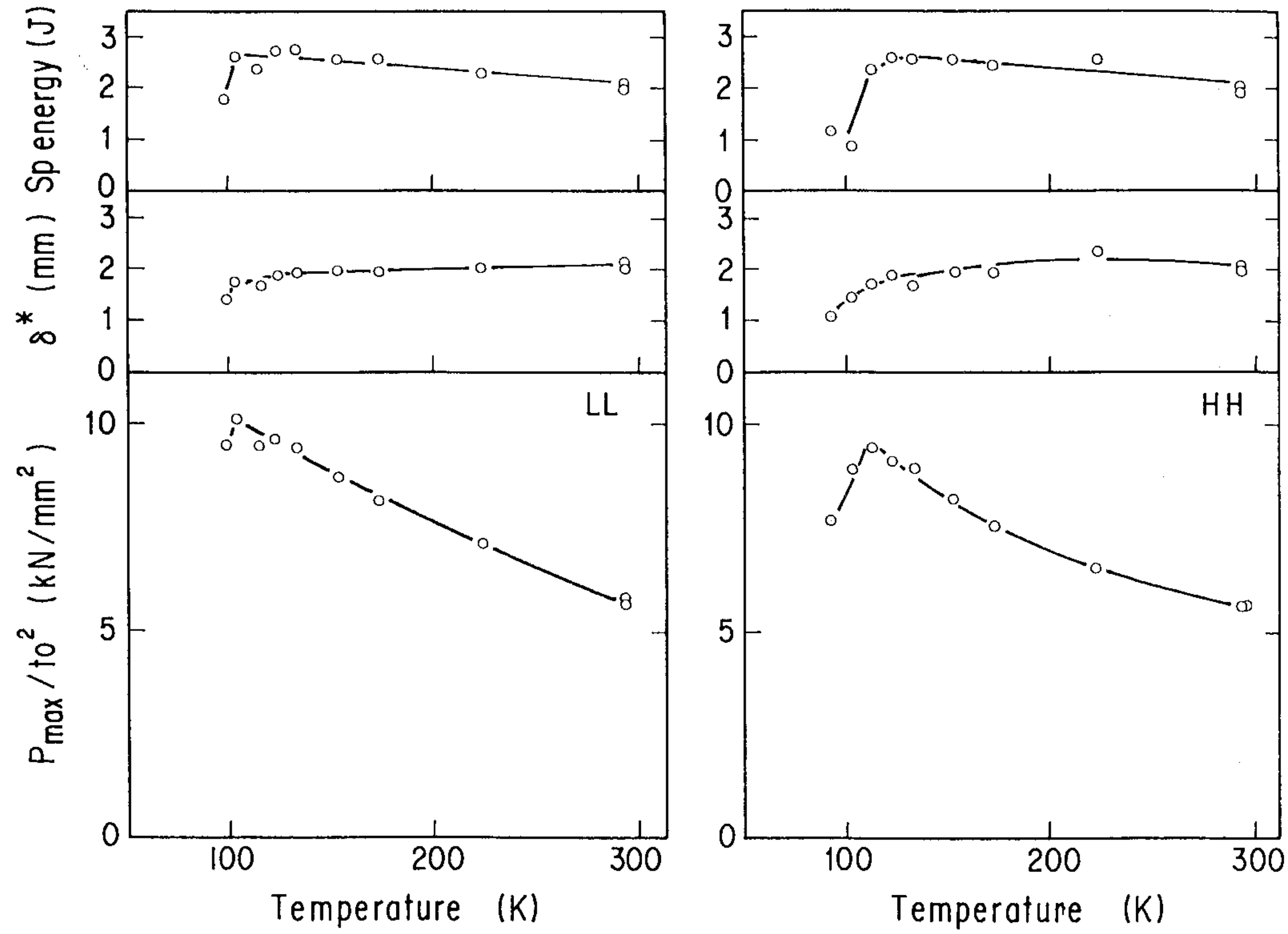

Appendix Fig. 3 SP-related parameters as a function of test temperature for 2 1/4Cr-1Mo steel (LL, HH).

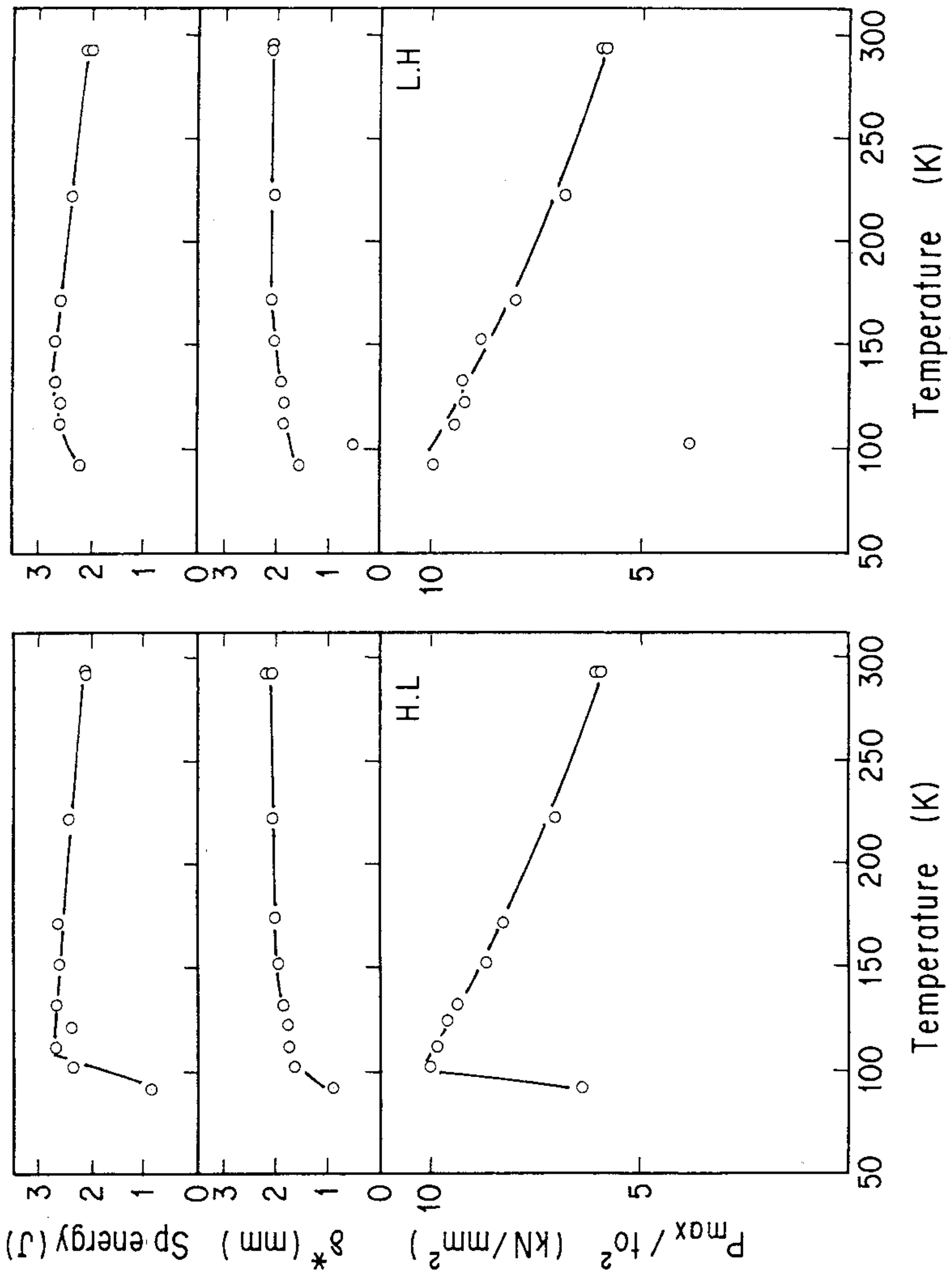

Appendix Fig. 4 SP-related parameters as a function of test temperature for 2 1/4Cr-1Mo steel (HL, LH).

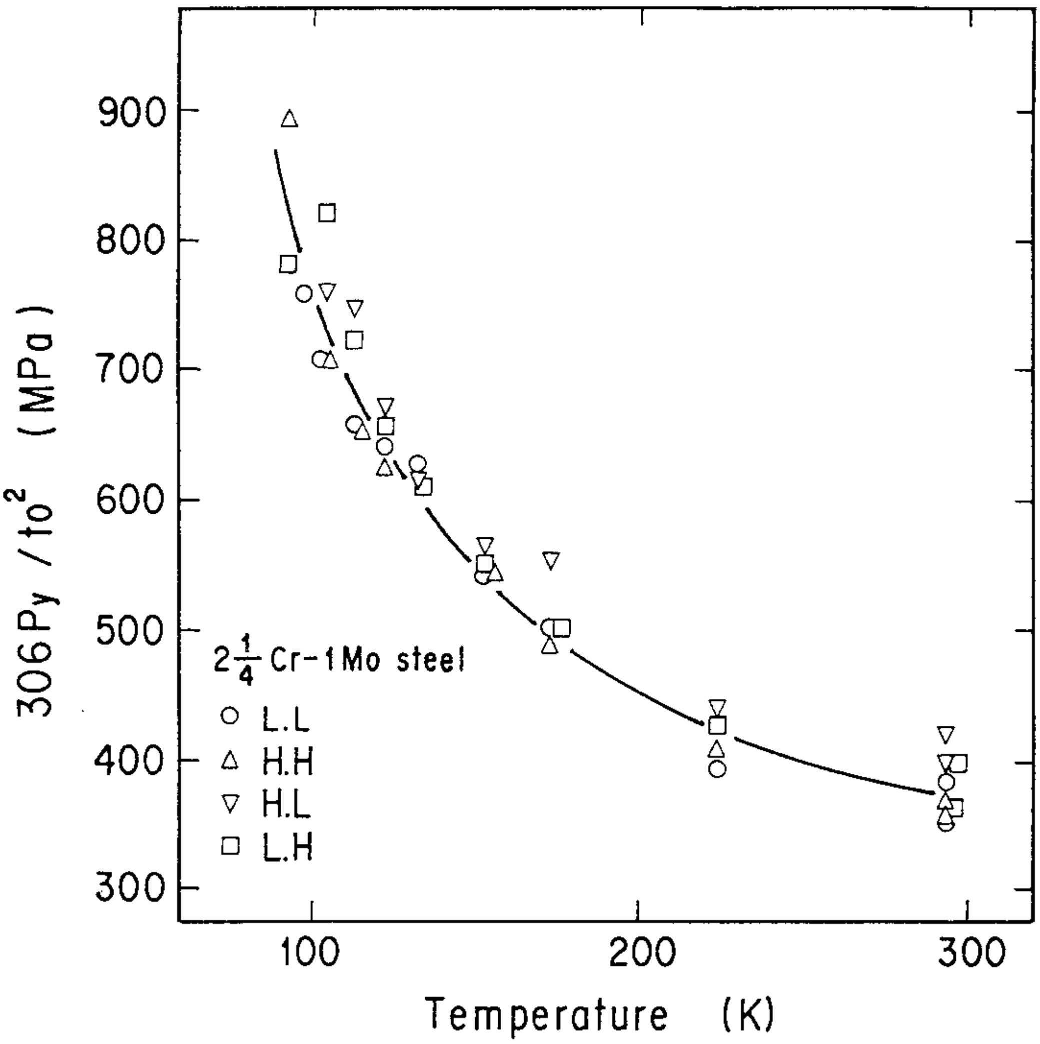

Appendix Fig. 5 SP-related parameters as a function of test temperature for 2 1/4Cr-1Mo steel (LL, HH, HL, LH).

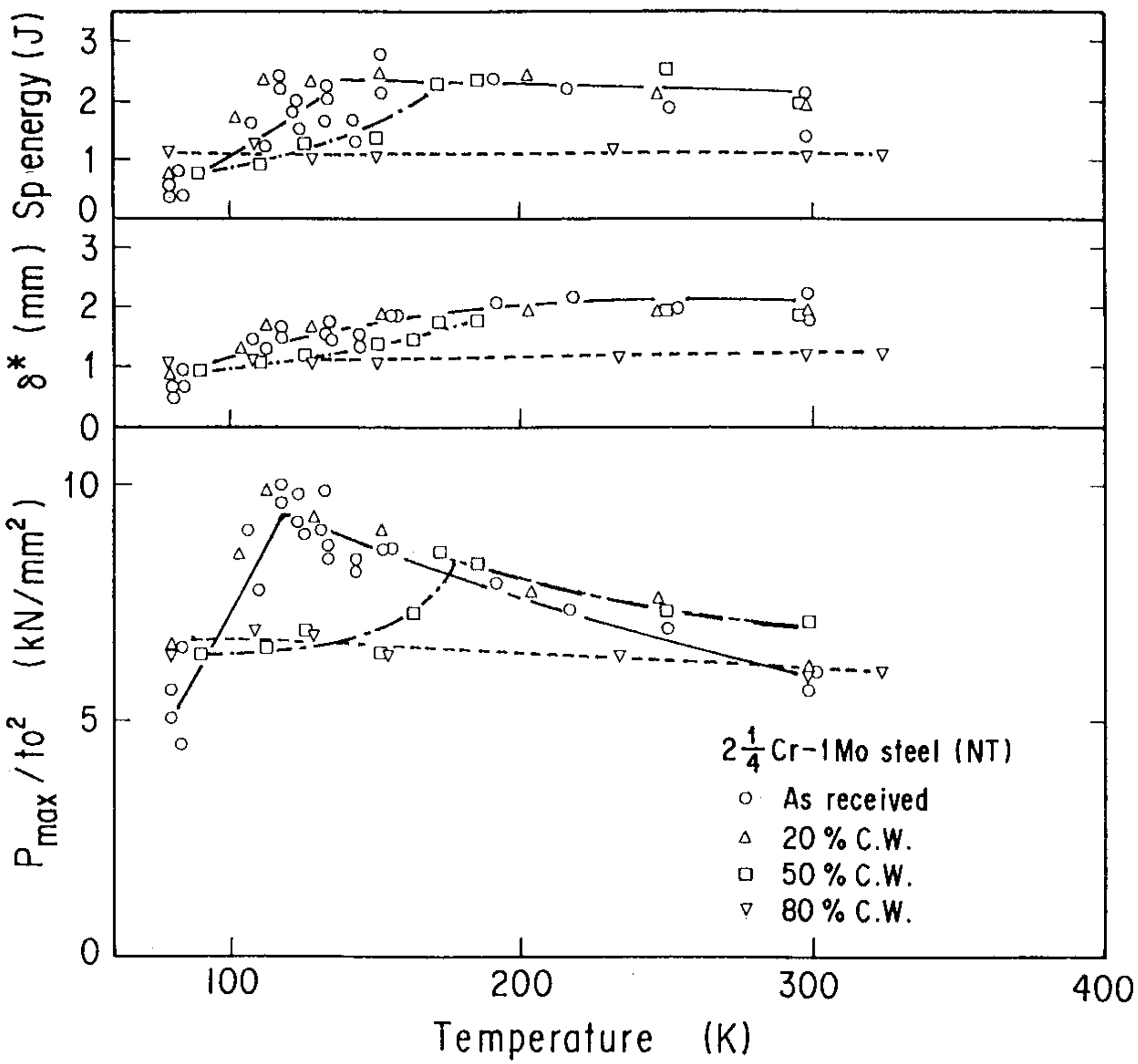

Appendix Fig. 6 SP-related parameters as a function of test temperature for 2 1/4Cr-1Mo steel (cold worked).

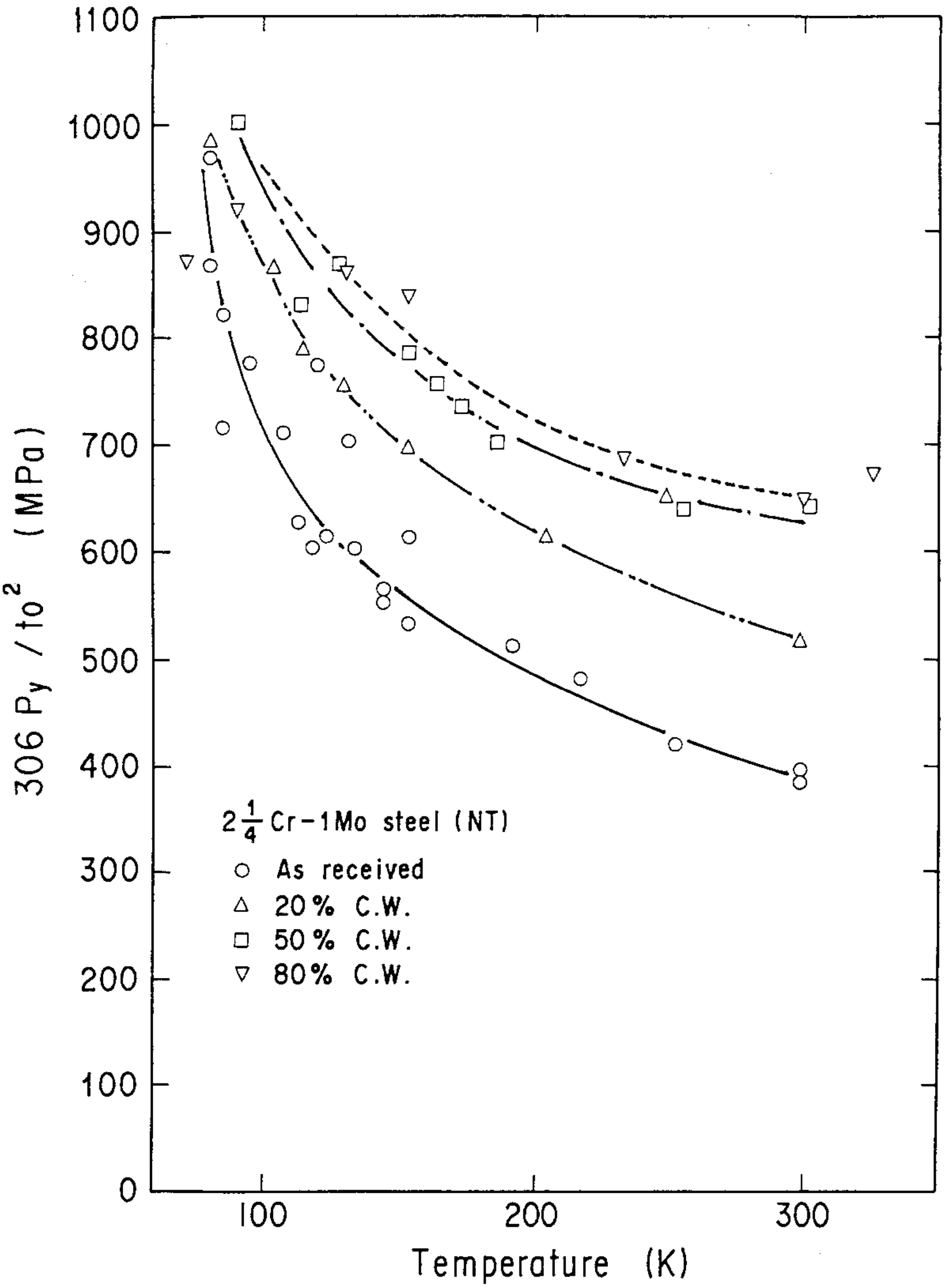

Appendix Fig. 7 SP-related parameters as a function of test temperature for 2 1/4Cr-1Mo steel (cold worked).

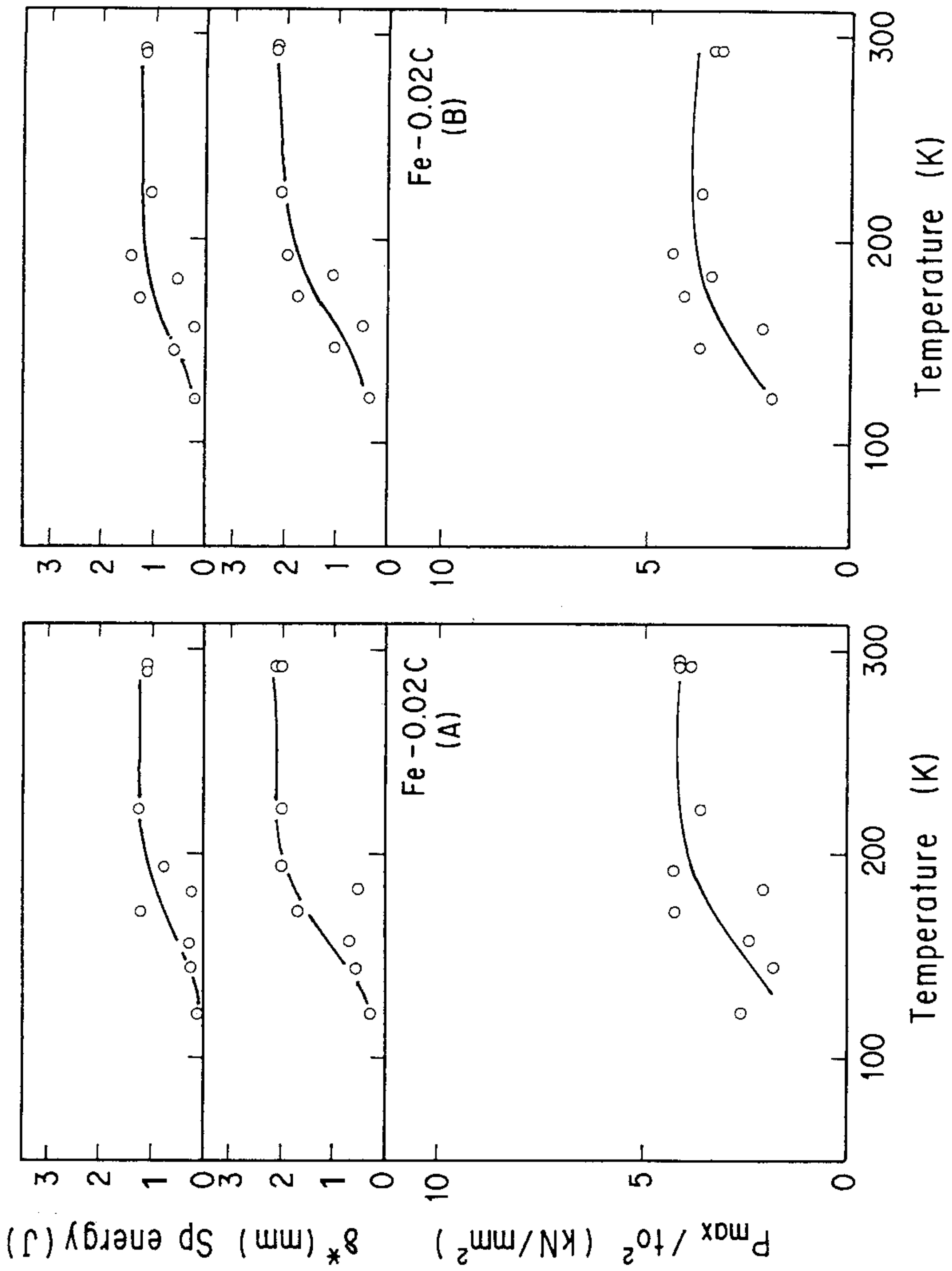

Appendix Fig. 8 SP-related parameters as a function of test temperature for 2 1/4Cr-1Mo steel (Fe-0.02C (A), Fe-0.02C-0.03P (B)).

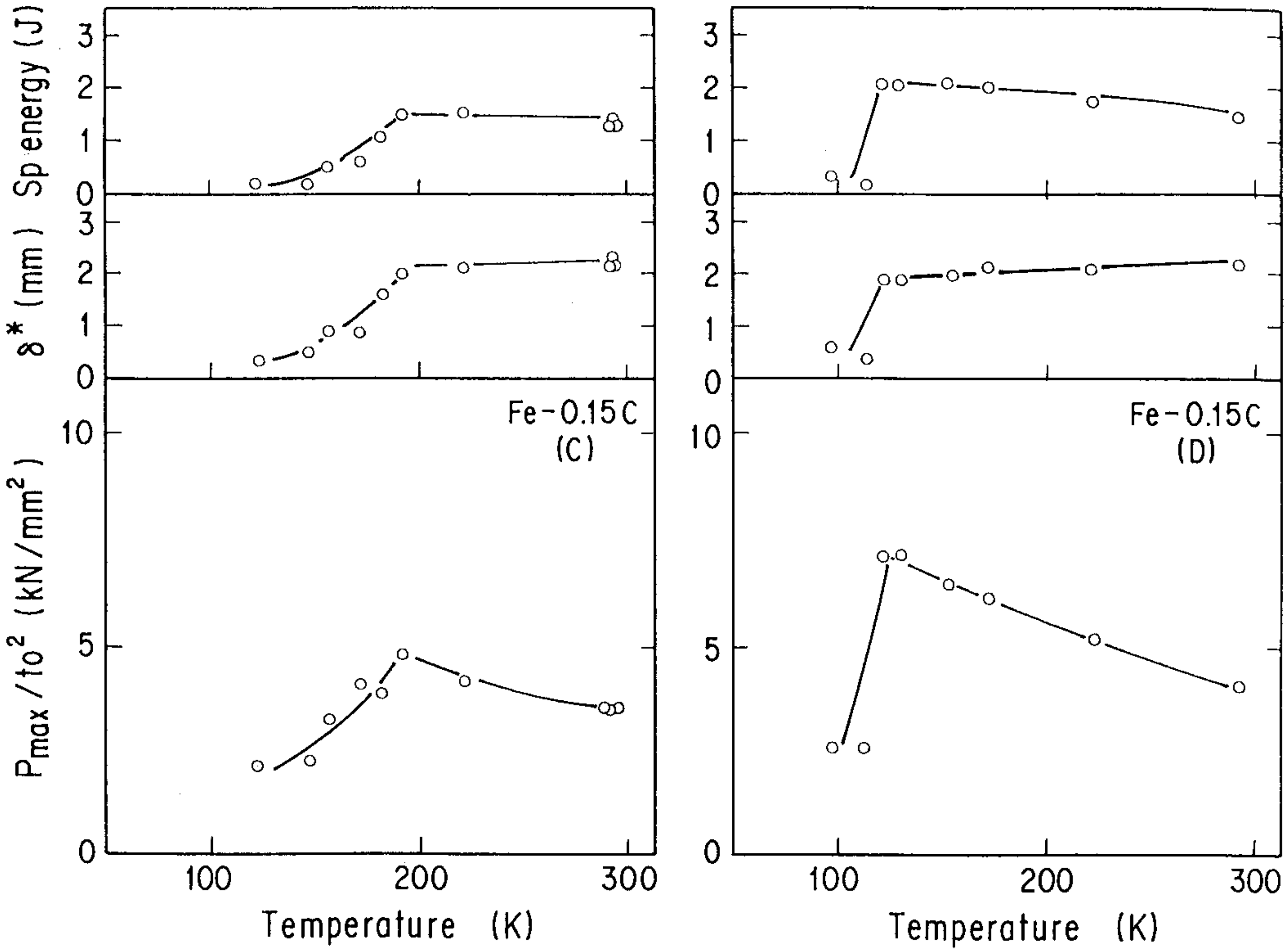

Appendix Fig. 9 SP-related parameters as a function of test temperature for 2 1/4Cr-1Mo steel (Fe-0.15C-0.03P (C), Fe-0.15C-0.03P (D)).

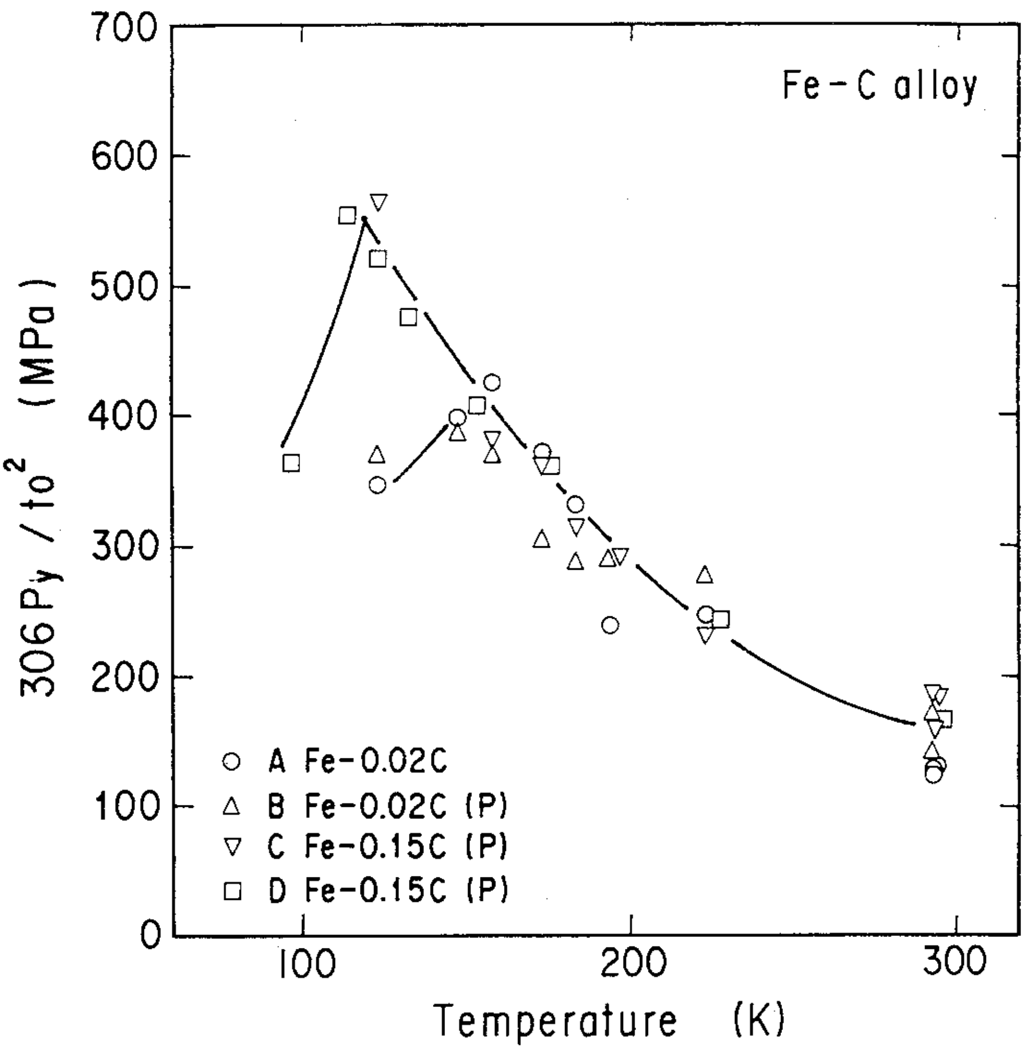

Appendix Fig. 10 SP-related parameters as a function of test temperature for 2 1/4Cr-1Mo steel (Fe-0.02C (A), Fe-0.02C-0.03P (B), Fe-0.15C -0.03P (C), Fe-0.15C-0.03P (D)).

Appendix Fig. 11

Fracture appearance of SP specimens;

Material: A387 Gr.22 Cl.2 (produced in the year S52)
20%(G) , 50%(F) , 80%(E) cold worked

Test temperature: -193℃ ～ 51℃

Specimen: 10x10x0.5(mm)

Comments: Irradiation tests corresponding to these materials:
NONE

A387Gr. 22 Cl. 2

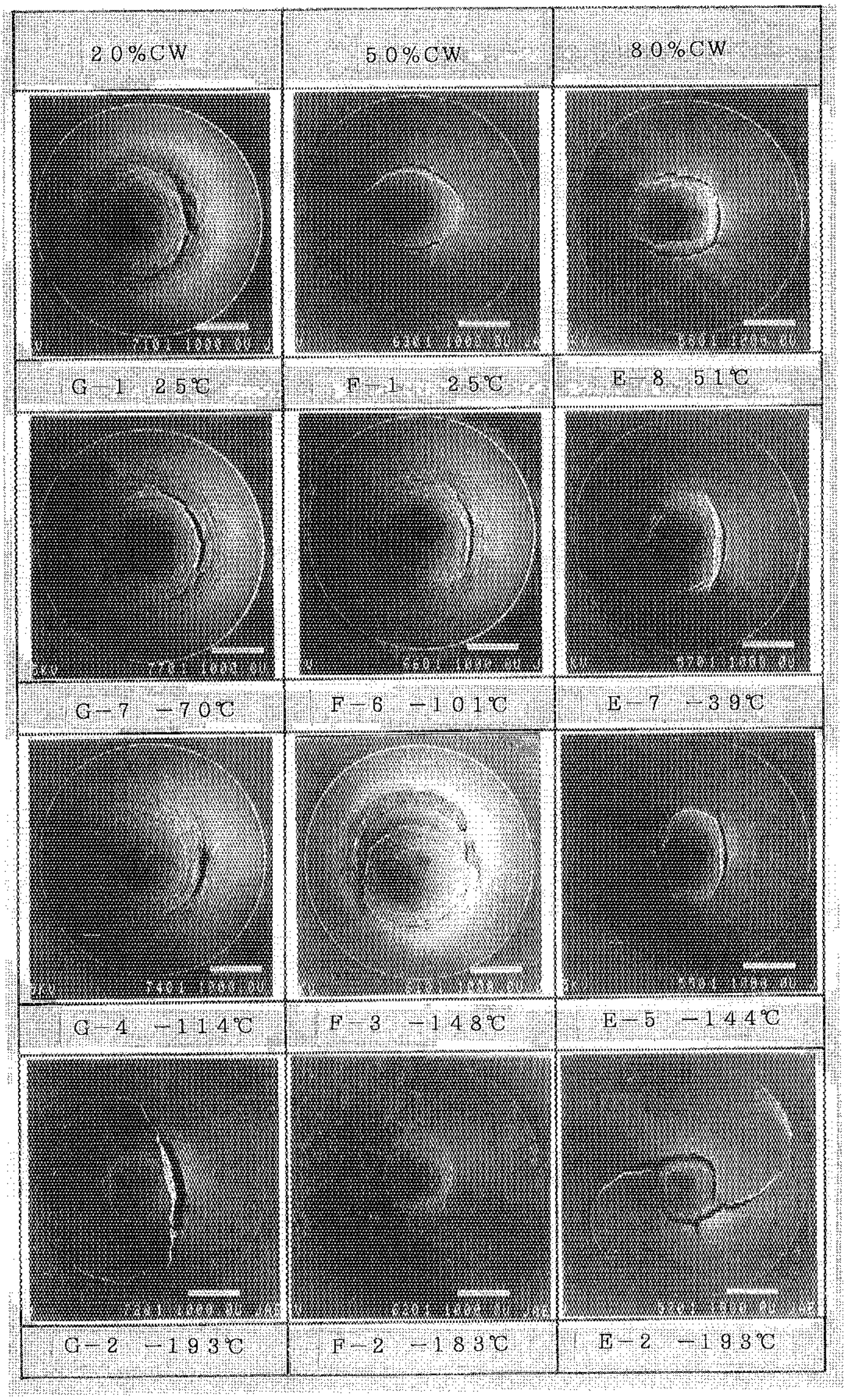

Appendix Fig. 11 Fracture appearance of SP specimens

Appendix Fig. 12

Fracture appearance of SP specimens;

Material: (1) A387 Gr.22 Cl.1 (produced in the year S52) :AN
(2) A387 Gr.22 Cl.2 (produced in the year S52) :A
(3) After aging (450℃x50000h) for material (2) :B

Test temperature: -180℃ ～ 25℃

Specimen: 10x10x0.5(mm)

Comments: Irradiation tests corresponding to these materials:

ICM-89H ((1),(2) and 10000h aged material)
90M-6A ((1),(2))
ICM-104H ((1),(2))

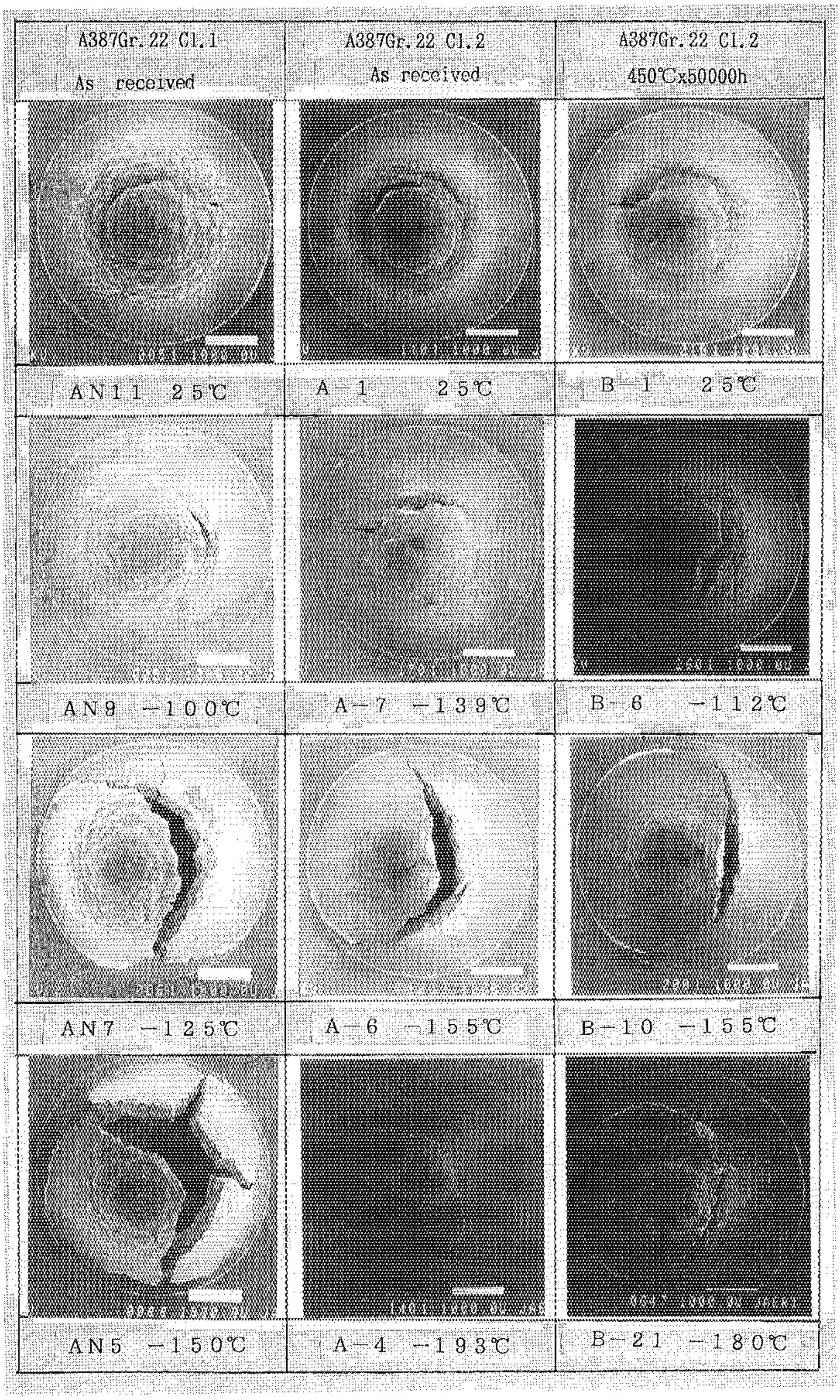

Appendix Fig. 12 Fracture appearance of SP specimens

Appendix Fig. 13

Fracture appearance of SP specimens;

Material: (1) Fe-0.02C model alloy :A
(2) Fe-0.02C-0.03P model alloy :B
(3) Fe-0.15C-0.03P model alloy (AN) :C
(4) Fe-0.15C-0.03P model alloy (QT) :D

Test temperature: -160℃ ～ 25℃

Specimen: 10x10x0.5(mm)

Comments: Irradiation tests corresponding to these materials:

ICM-96H ((1), (2), (3), (4))

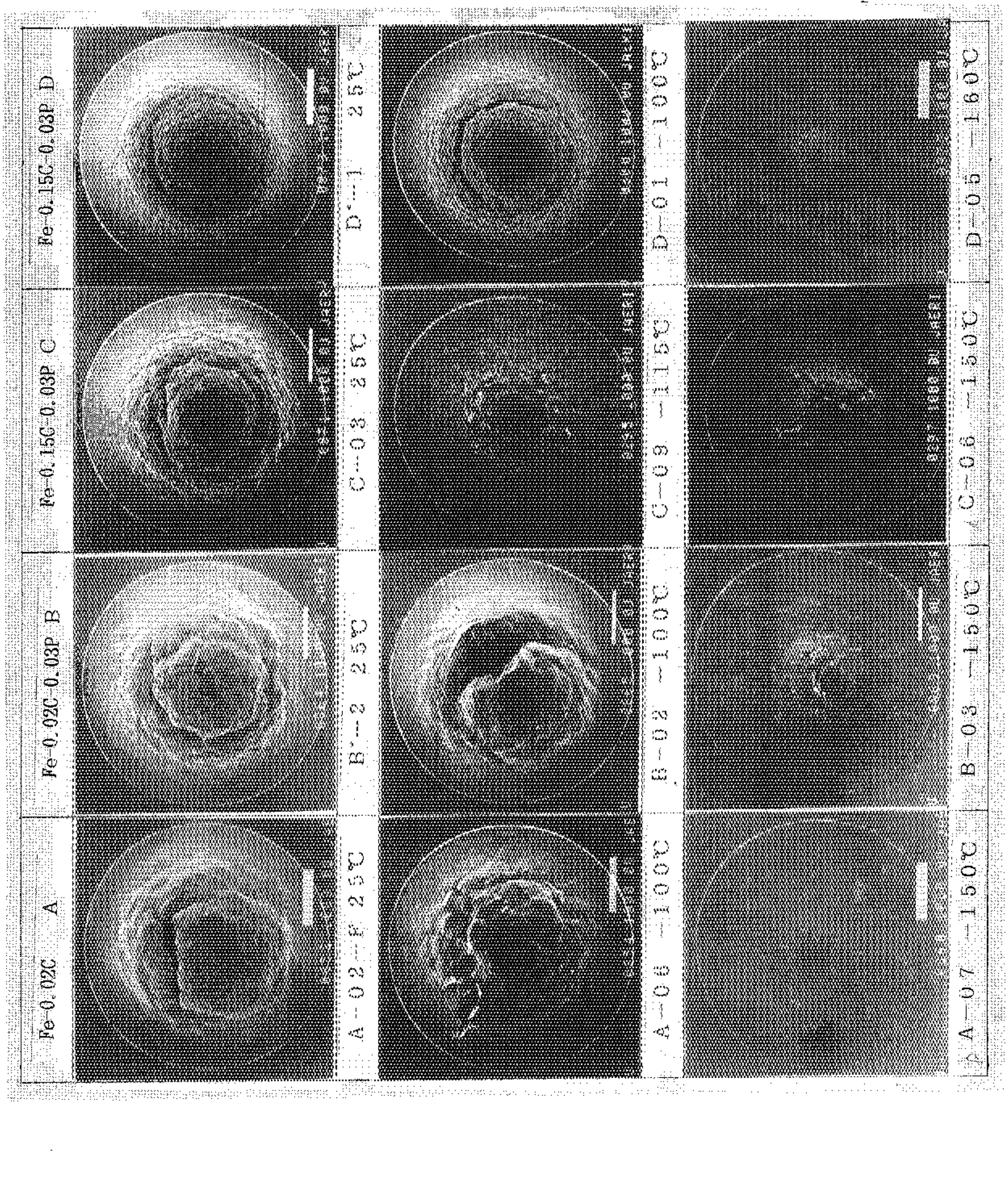

Appendix Fig. 13 Fracture appearance of SP specimens

Appendix Fig. 14

Fracture appearance of SP specimens;

Material: (1) A387 Gr.22 Cl.2 experimantal alloy (0.005P,0.01Cu) :LL,4
(2) A387 Gr.22 Cl.2 experimantal alloy (0.01P,0.05Cu) :HH,5
(3) A387 Gr.22 Cl.2 experimantal alloy (0.01P,0.01Cu) :HL,6
(4) A387 Gr.22 Cl.2 experimantal alloy (0.005P,0.01Cu) :LH,7

Test temperature: -180℃ ～ 25℃

Specimen: 10x10x0.5(mm)

Comments: Irradiation tests corresponding to these materials:

ICM-96H ((1),(2),(3),(4))

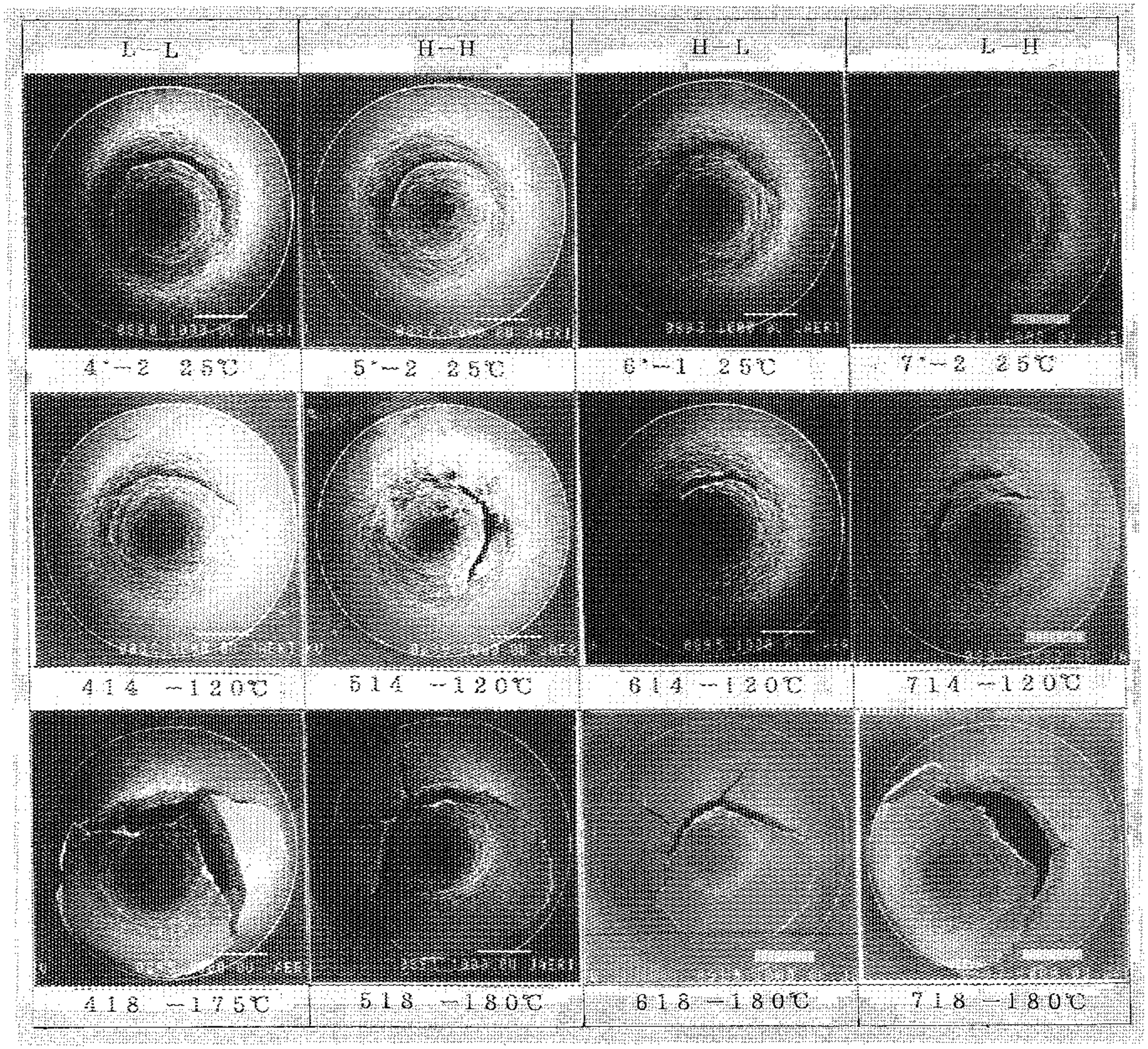

Appendix Fig. 14 Fracture appearance of SP specimens

Appendix Fig. 15

Fracture surface of SP specimens; observation area C (in Fig.9)

Material: A387 Gr.22 Cl.2
20%(G), 50%(F), 80%(E) cold worked
Test temperature: -193℃ ~ 25℃

Specimen: 10x10x0.5(mm)

Comments: Irradiation tests corresponding to these materials:

NONE

Appendix Fig. 15

Fracture surface of SP specimens; observation area C (in Fig. 9)

Material: A387 Gr. 22 Cl. 2
20%(G), 50%(F), 80%(E) cold worked
Test temperature: -193℃ ~ 25℃

Specimen: 10x10x0.5(mm)

Comments: Irradiation tests corresponding to these materials:

NONE

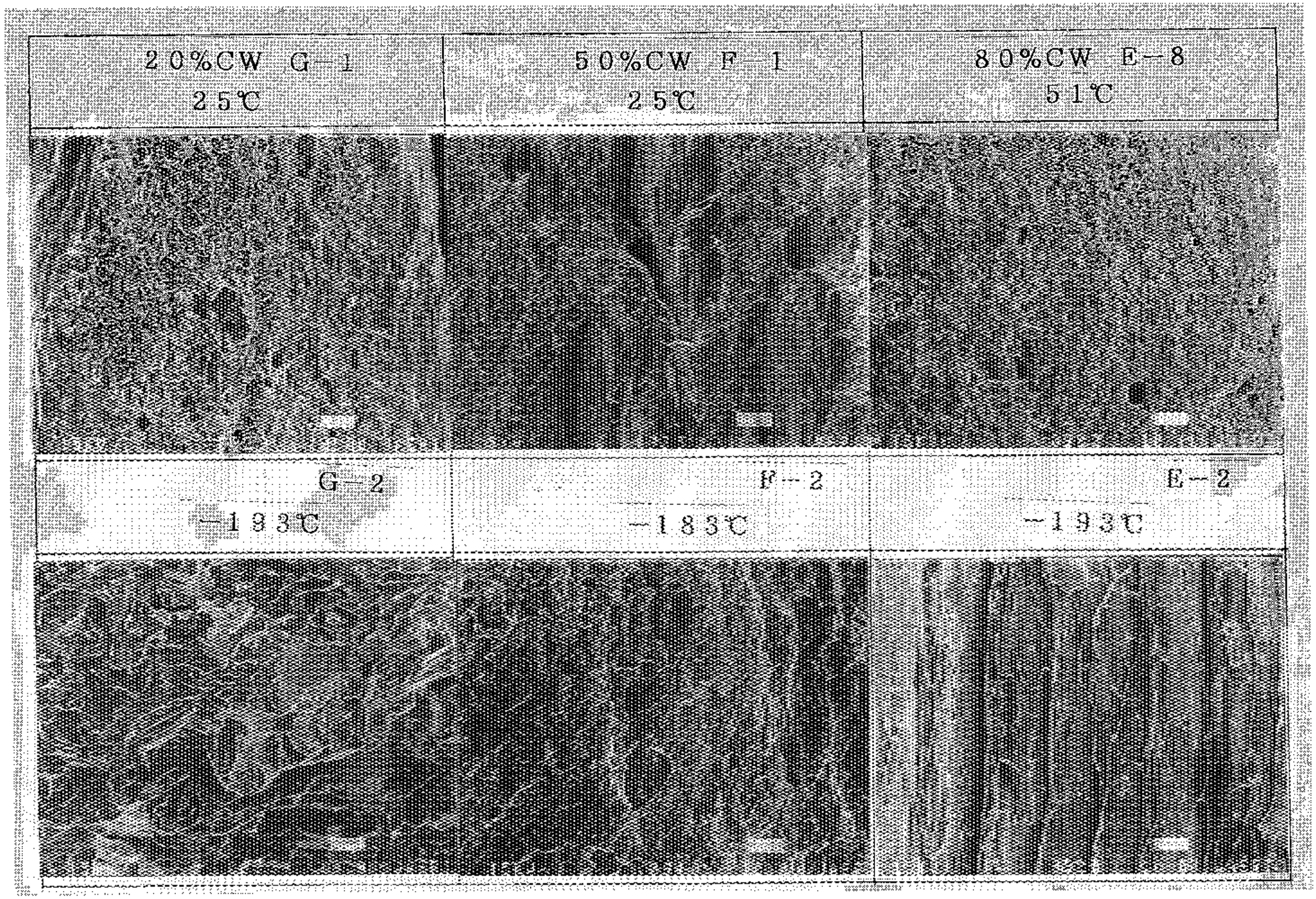

Appendix Fig. 15 Fracture surface of SP specimens; observation area C (in Fig. 9)

Appendix Fig. 16

Fracture surface of SP specimens; observation area C (in Fig.9)

Material: (1) Fe-0.02C model alloy :A
(2) Fe-0.02C-0.03P model alloy :B, B*
(3) Fe-0.15C-0.03P model alloy (AN) :C
(3) Fe-0.15C-0.03P model alloy (QT) :D
Test temperature: -180℃ ～ 25℃

Specimen: 10x10x0.5(mm)

Comments: Irradiation tests corresponding to these materials:

ICM-96H ((1),(2),(3),(4))

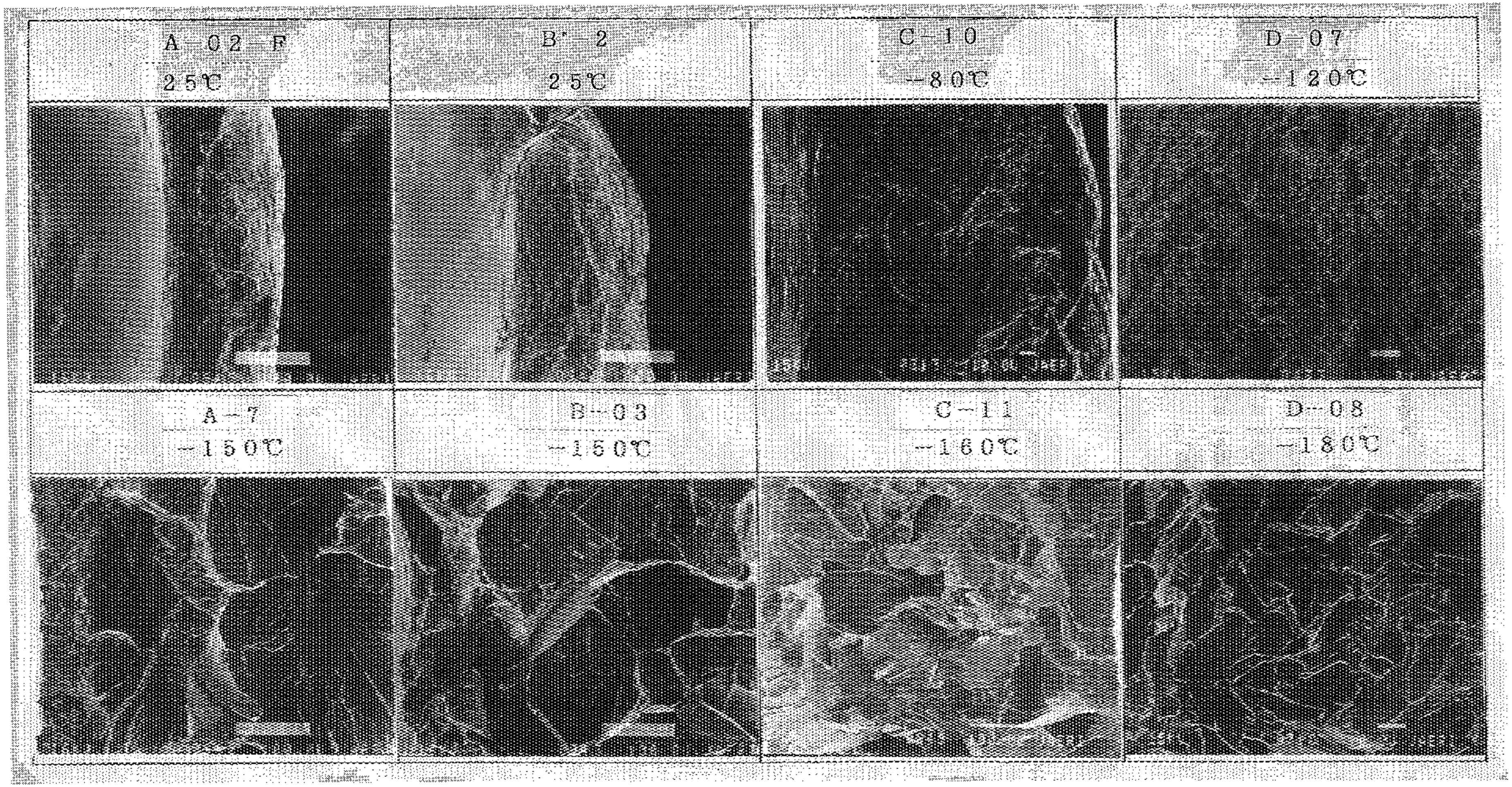

Appendix Fig. 16 Fracture surface of SP specimens; observation area C (in Fig. 9)

Appendix Fig. 17

Fracture surface of SP specimens; observation area C (in Fig. 9)

Material:	(1) A387 Gr.22 Cl.1 (produced in S52)	:AN
	(2) Fe-0.02C model alloy	:A
	(3) Fe-0.02C-0.03P model alloy	:B
	(4) A387 Gr.22 Cl.2 experimantal alloy (0.01P, 0.05Cu)	:5, HH

Test temperature: -180℃ ～ 25℃

Specimen: 10x10x0.5(mm)

Comments: Irradiation tests corresponding to these materials:

ICM-89H ((1))
90M-6A ((1))
ICM-96H ((2), (3), (4))
ICM-104H ((1))

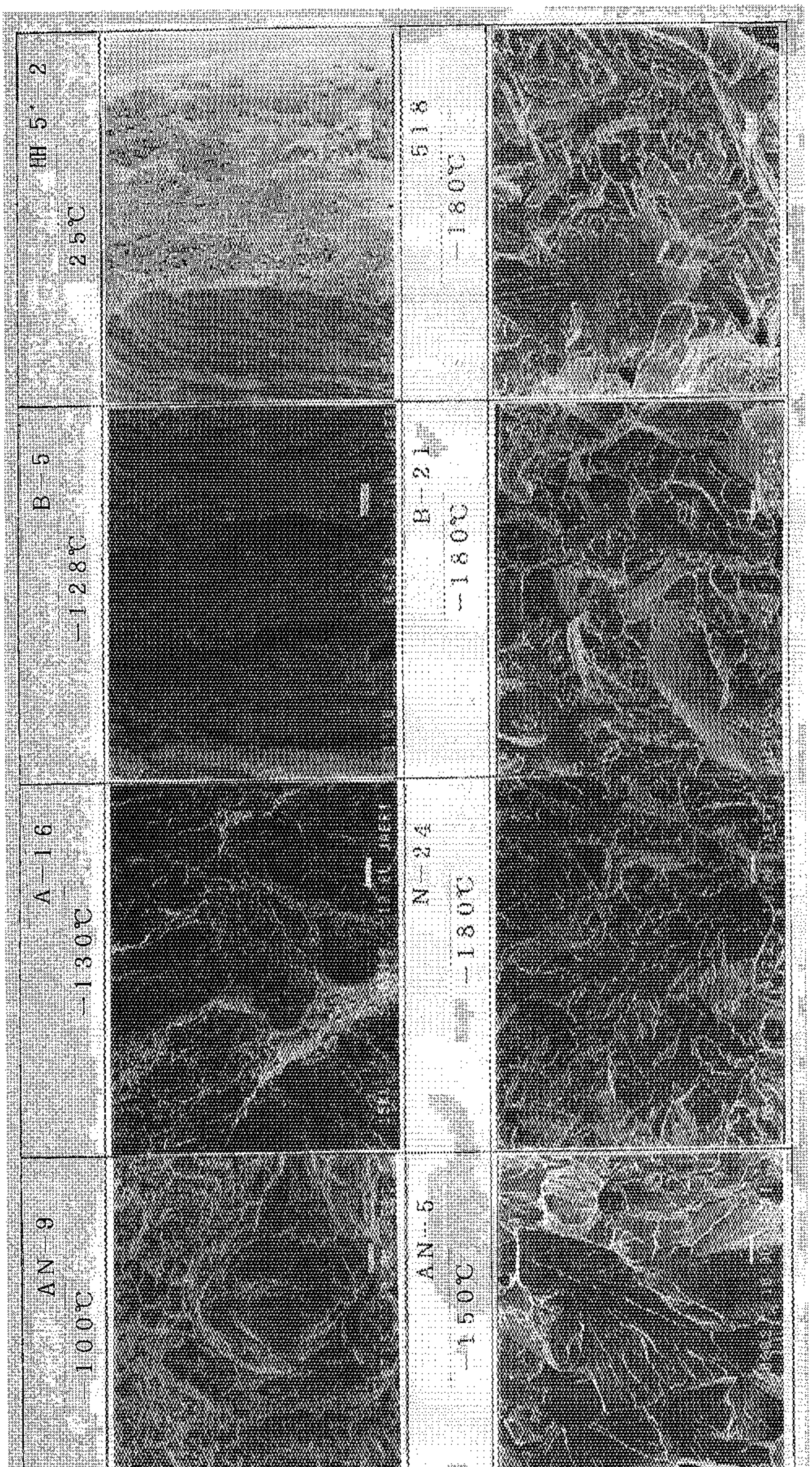

Appendix Fig. 17 Fracture surface of SP specimens; observation area C (in Fig. 9)